The Use of Electrochemical Techniques for the Characterization of the Corrosion Behavior of Sol-Gel-Coated Metals

60

Francesco Andreatta and Lorenzo Fedrizzi

Contents

F. Andreatta (✉) · L. Fedrizzi
Polytechnic Department of Engineering and Architecture, University of Udine, Udine, Italy
e-mail: francesco.andreatta@uniud.it

© Springer International Publishing AG, part of Springer Nature 2018

L. Klein et al. (eds.), *Handbook of Sol-Gel Science and Technology*,
https://doi.org/10.1007/978-3-319-32101-1_144

Abstract

Deposition of sol-gel coatings is a promising method for corrosion protection of metal substrates. As an example, sol-gel coatings represent an alternative to the use of chromate conversion coatings for protection of aluminum alloys in the aerospace industry. In order to expand the use of sol-gel coatings, it is important to assess their corrosion behavior. The sol-gel coating should provide an efficient barrier against aggressive species limiting corrosion of the metal substrate. Moreover, the coating should offer the possibility to incorporate corrosion inhibitors in order to provide active behavior to the coating. The sol-gel coating should be well adherent to the base metal and should also promote the adhesion of organic primer and topcoat when the sol-gel coating is employed as a pretreatment of the substrate.

This chapter focuses on the use of electrochemical methods for the characterization of corrosion properties of thin sol-gel coatings. Barrier properties, effect of corrosion inhibitors incorporated in the sol-gel coatings, and adhesion promotion are targeted in this chapter providing selected examples taken from our scientific work.

Introduction

Aluminum alloys are protected with a complex paint system consisting of conversion layer, primer, and topcoat. Cr-based pretreatments are extensively employed as conversion coatings because they provide very good adhesion for primer and topcoat associated with good barrier properties (Metroke et al. 2001). Moreover, chromate conversion coatings exhibit self-healing ability (Metroke et al. 2001). However, the use of chromate conversion coatings is restricted, and alternative pretreatments should be employed for aluminum alloys (Metroke et al. 2001; di Maggio et al. 2001; Bethencourt et al. 1998; Osborne 2001). The sol-gel technique can be employed for the production of oxide films on different metal substrates (Metroke et al. 2001; Osborne 2001; Guglielmi 1997; Ballard et al. 2001; Metroke and Apblett 2004). A wide range of metal alkoxides or salts can be used as precursors for the oxide synthesis. The coating undergoes hydrolysis and condensation to form a continuous oxide structure during the deposition procedure. Sol-gel technology enables formation of highly adherent, chemically inert oxide films on metal substrates. Moreover, it is possible to deposit thin films of submicrometer thickness or thicker films through application of multiple layers by controlling deposition parameters like withdraw rate in the case of dip coating technology (Metroke et al. 2001). The wide variety of sol-gel precursor materials commercially available enables preparation of several combinations of high-purity and single- and multicomponent oxide materials. Incorporation of water- and alcohol-soluble dopant ions is also possible increasing the versatility of the sol-gel method. The development of non-chromated coating systems for aluminum alloys has been targeted with the attempt to replace chromate conversion coating with a thin sol-gel layer (typically

50–200 nm) (Osborne et al. 2001). This approach is very promising because sol-gel coating systems are usually thick (in the micrometer range) and are generally regarded as complete coating systems. The superior adhesion behavior of thin Zr- and Si-based sol-gel films relative to chromate conversion coatings is the main advantage of developing thin coatings.

Corrosion protection of different types of sol-gel coatings has been extensively investigated in the past (Metroke et al. 2001). Oxide layers deposited by dip coating and spin coating from sol-gel systems improve the corrosion resistance of aluminum alloys (Metroke et al. 2001; Voevodin et al. 2001). Silane-based sol-gel coatings are reported to improve resistance of aluminum to general and localized corrosion (Beccaria et al. 1999; Beccaria and Chiaruttini 1999). Moreover, mixed SiO_2 and ZrO_2 oxide layers deposited on AA2024 with sol-gel technique increased resistance to localized attack (Yang et al. 2001). Zr-based sol-gel coatings can be used as barrier layers in paint systems for AA2024 (Voevodin et al. 2005). Barrier properties and long-term corrosion resistance need to be improved in order to substitute chromate conversion coatings with thin sol-gel films. Our research group followed the strategy of developing thin sol-gel coatings for different aluminum alloys (Andreatta et al. 2007, 2008, 2010a, b, 2011; Paussa et al. 2010a, b, 2012).

Background on Electrochemical Techniques

Corrosion is an electrochemical process that requires anodes and cathodes in electrical contact and an ionic conduction path through an electrolyte (Sheir et al. 1994; Fontana 1986; Bard and Faulkner 2001). The electrochemical process leads to electron flow between the anodes and the cathodes. The rate of the electron flow corresponds to the rates of the oxidation and reduction reactions taking place on the metal surface. The corrosion process is related to thermodynamic considerations since the free-energy change and, in particular, its sign indicate whether the electrochemical process is spontaneous. According to mixed potential theory, any net electrochemical reaction can be divided into two or more oxidation and reduction reactions, and there can be no net electrical charge accumulation. Based on the concept of half cell potentials (Fontana 1986), the most negative (or active) half cell tends to be oxidized, while the most positive (or noble) half cell tends to be reduced in any electrochemical reaction. Thus, corrosion processes will occur on the metal surface only if the spontaneous direction of the electrochemical reaction indicates metal oxidation. It is important to underline that thermodynamic considerations do not provide information about the rate of corrosion processes. If an oxidation process proceeds at a very low rate, the metal will be inert and corrosion will not be relevant. This indicates that the kinetics of corrosion processes and the determination of the corrosion rate of a corroding metal play a very important role in the field of corrosion protection.

Electrochemical techniques have been developed to obtain information about the kinetics of corrosion processes (corrosion rate) and about corrosion mechanisms. Several textbooks cover the application of electrochemical methods in corrosion

studies (Fontana 1986; Sheir et al. 1994; Bard and Faulkner 2001; Kelly et al. 2002). This chapter recalls the most important concepts about electrochemical cells and the main electrochemical techniques employed for the study of metals coated with sol-gel films.

Open Circuit Potential Measurements

In a corroding system in the absence of applied potential (open circuit condition), the oxidation of the metal and the reduction of some species in solution (like oxygen) occur simultaneously at the metal/electrolyte interface. Under these circumstances, the net measurable current is zero. The open circuit potential of the corroding metal is measured in the absence of applied potential as the potential difference between the metal and a reference electrode using a high-impedance voltmeter. Since oxidation and reduction processes occurring at the metal/electrolyte interface might change with time, it follows that the measured open circuit potential varies as a function of the immersion time in the electrolyte. The measurement of the open circuit potential of a corroding metal can provide information about oxidation or reduction processes taking place on the metal surface. Moreover, the open circuit potential can be used to predict the behavior of the metal in the case of galvanic coupling with other metals. In the case of coated metals, the open circuit potential can provide information about the presence of defects in the coating.

Potentiodynamic Polarization

Polarization techniques are based on the external application of a potential to the system in order to obtain a net oxidation (anodic polarization) or reduction (cathodic polarization) process at the metal/electrolyte interface. The potential may be held constant or may be varied with time in a predetermined manner as the current is measured as a function of time or potential. The most commonly used techniques are as follows:

- Determination of the potential-current density relationship during polarization at constant potential (potentiostatic polarization). The current density is the experimentally measured variable.
- Determination of the potential-current density relationship during polarization with potential changed continuously at a predetermined sweep rate (potentiodynamic polarization).

Electrochemical polarization methods can be used to determine corrosion rates according to the method introduced by Stern-Geary (Sheir et al. 1994). The method in spite of its limitations has a number of significant advantages and can be used for rapidly monitoring the instantaneous corrosion rate of a corroding system. Moreover, polarization methods can be employed for the investigation of uniform

corrosion, susceptibility to bimetallic corrosion, pitting, intergranular attack, and stress-corrosion cracking and for the study of corrosion inhibitors. In the case of coated metals, polarization techniques enable the study of the protection level guaranteed by the coating.

Electrochemical Impedance Spectroscopy

Measurements of the electrical impedance by the imposition of an alternating potential of known frequency can provide information on the nature of a corroding surface. This type of measurement is known as electrochemical impedance spectroscopy, and it is a well-established technique for investigating the electrochemical behavior of different bare and coated systems. The electrochemical impedance is a fundamental characteristic of the electrochemical system. The knowledge of the frequency dependence of impedance for a corroding system enables a determination of an appropriate equivalent electrical circuit describing that system. Such a circuit is typically constructed from resistors and capacitors. As an example, the electrical double layer originating at the metal/electrolyte interface of a corroding metal may be regarded as a resistance and capacitance in parallel (Sheir et al. 1994). Polarization techniques discussed above often drive the metal under investigation to a condition far from equilibrium. In contrast, the approach of electrochemical impedance spectroscopy is to perturb the cell with an alternating signal of small magnitude and to observe the way in which the system follows the perturbation at steady state. Among the most important advantages of this approach are that there is the experimental ability to make high-precision measurements because the response may be indefinitely steady and the possibility to perform measurements over a wide time (or frequency) range (Bard and Faulkner 2001). This aspect is very important for coated metals, since it is possible to evaluate the protective properties of a coating as a function of the immersion time in an aggressive electrolyte.

Electrochemical Cells and Potentiostat

In order to carry out the different measurements described above, it is necessary to employ an electrochemical cell (Sheir et al. 1994; Bard and Faulkner 2001). The electrochemical cell consists of the working electrode (the sample of interest), the reference electrode (used to measure the potential of the working electrode), and the counter electrode (used to apply current to the working electrode).

A potentiostat is used to control the voltage across the working electrode–counter electrode pair, and it adjusts this voltage to maintain the potential difference between the working and reference electrodes (which it senses through a high-impedance feedback loop). The potentiostat is an active element whose function is to force through the working electrode the current required to achieve the desired potential at any time.

Impedance measurements in the frequency domain are carried out with a frequency response analyzer (FRA). The FRA generates an alternating potential signal of small magnitude which is fed to the potentiostat. This is added to the open circuit potential of the system and fed to the cell. The resulting current, or more precisely a voltage signal proportional to the current, is fed to the analyzer, mixed with the input signal, and integrated over several signal periods to yield signals that are proportional to the real and imaginary parts of the impedance (or equivalently the magnitude and phase angle of the impedance).

Morphology and Electrochemical Behavior of Sol-Gel Films on Aluminum Alloys

Sol-Gel Films Employed as Pretreatments Before Painting Aluminum Alloys

This section discusses the use of thin ZrO_2 sol-gel films as pretreatment for AA2024-T3 aluminum alloy (Andreatta et al. 2010a, 2011). The substrate was subjected to alkaline cleaning, alkaline etching, and acid desmutting before deposition of ZrO_2 films. The deposition of the ZrO_2 pretreatment was carried out using two different precursor solutions. The first was a solution of metal–organic precursor, which was 0.1 M or 0.6 M $Zr(OBu^n)_4$ in anhydrous n-butanol. The second was an aqueous solution of an inorganic precursor. This was $0.4MZrO(NO_3)_2$ in water. The deposition was performed by dipping technique for both application routes. Two overlapping ZrO_2 layers were applied on AA2024-T3 samples. After each dip in the sol-gel solution, the samples were subjected to thermal treatment at 150 °C for 4 min followed by drying at room temperature. Details about the procedure for the deposition of the sol-gel films are reported elsewhere (Andreatta et al. 2011).

Deposition of Pretreatments from Solution of Metal–Organic Precursor

Figure 1 shows a typical surface morphology of AA2024-T3 after surface preparation consisting of alkaline degreasing and alkaline and acid etching in order to remove intermetallics and the defected oxide layer resulting from cold rolling. The procedure followed for surface preparation prior deposition of sol-gel films leads to nonuniform attack due to the inhomogeneous microstructure of AA2024-T3 alloy. Several craters with 5–10 μm size can be recognized on the substrate. It is likely that craters are generated by the removal of intermetallics during alkaline etch. The development and optimization phase of deposition of sol-gel films on AA2024-T3 substrate carefully considered the effect of surface preparation since this might represent a critical step for the deposition of sol-gel films by dipping and spraying technology. However, it should be considered that the existence of craters due to surface preparation cannot be completely avoided since the removal of defected

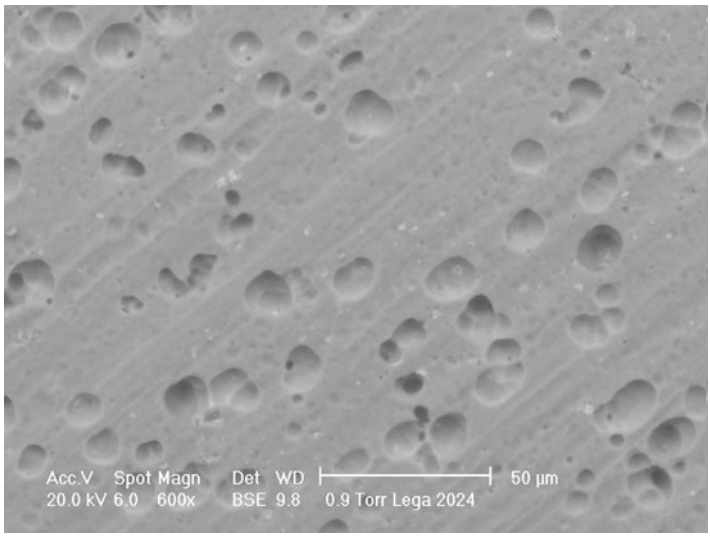

Fig. 1 SEM micrograph of AA2024-T3 after surface preparation consisting of alkaline degreasing, alkaline etching, and acid etching (Reprinted from Prog Org Coatings, 72, Andreatta F, Paussa L, Lanzutti A, Rosero Navarro NC, Aparicio M, Castro Y, et al., Development and industrial scale-up of ZrO2 coatings and hybrid organic-inorganic coatings used as pre-treatments before painting aluminium alloys, 3–14, Copyright (2011), with permission from Elsevier)

oxide layer and intermetallic by etching is necessary in order to promote the deposition of a defect-free sol-gel film on the substrate.

Figure 2 shows a TEM micrograph of AA2024-T3 pretreated with a ZrO_2 sol-gel layer. Two layers of ZrO_2 were deposited on the substrate by dipping technology. The film appears uniform and continuous on the AA2024-T3 substrate. The film thickness is about 100 nm.

Figure 3 displays a SEM micrograph of AA2024-T3 coated with a ZrO_2 sol-gel layer. Although the film is very thin and transparent, the SEM micrograph reveals the structure of the film deposited on the substrate. Moreover, it can be recognized that the morphology of the pretreated alloy reveals the same features observed after surface preparation indicating that the ZrO_2 film tends to uniformly cover the microstructure generated during surface preparation. The SEM micrograph evidences a relatively large crater that is most likely completely coated by the sol-gel film since no evident defects can be seen at this location. In particular, cracks are not observed in the film covering the crater. It has been observed that craters like the ones visible in Fig. 3 are critical spots to be coated by dipping technique due to possible crack formation during film densification (thermal treatment). The SEM micrograph in Fig. 3 is relative to optimized deposition procedures, which targeted reduction of film defects in order to maximize barrier properties of the film. In general, optimized pretreatments for AA2024-T3 are nearly crack-free. In general, it can be stated that there is a more marked tendency to form cracks in the craters than

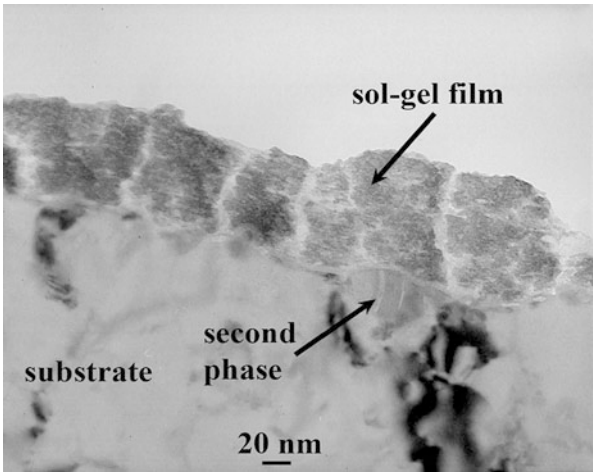

Fig. 2 TEM micrograph of AA2024-T3 pretreated with a ZrO_2 sol-gel layer deposited by dipping technology using 0.1 M solution of metal–organic precursor (two layers) (Reprinted from Prog Org Coatings, 72, Andreatta F, Paussa L, Lanzutti A, Rosero Navarro NC, Aparicio M, Castro Y, et al., Development and industrial scale-up of ZrO2 coatings and hybrid organic-inorganic coatings used as pre-treatments before painting aluminium alloys, 3–14, Copyright (2011), with permission from Elsevier)

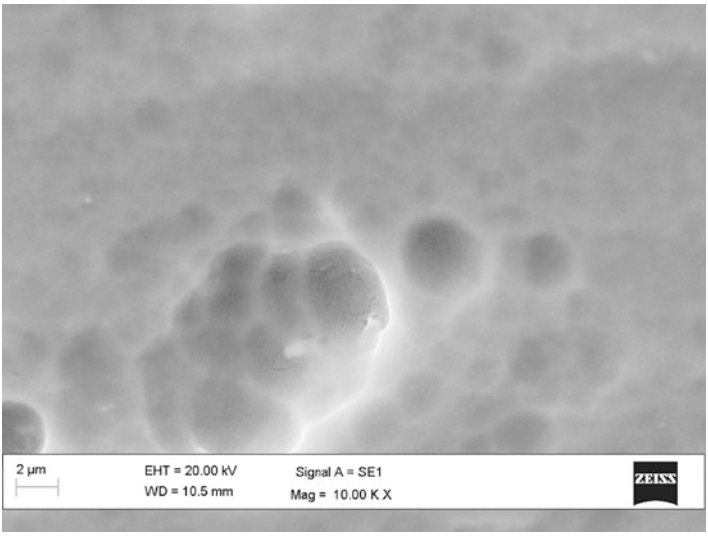

Fig. 3 SEM micrograph of AA2024-T3 pretreated with a ZrO_2 sol-gel layer deposited by dipping technology using 0.1 M solution of metal–organic precursor (three layers) (Reprinted from Prog Org Coatings, 72, Andreatta F, Paussa L, Lanzutti A, Rosero Navarro NC, Aparicio M, Castro Y, et al., Development and industrial scale-up of ZrO2 coatings and hybrid organic-inorganic coatings used as pre-treatments before painting aluminium alloys, 3–14, Copyright (2011), with permission from Elsevier)

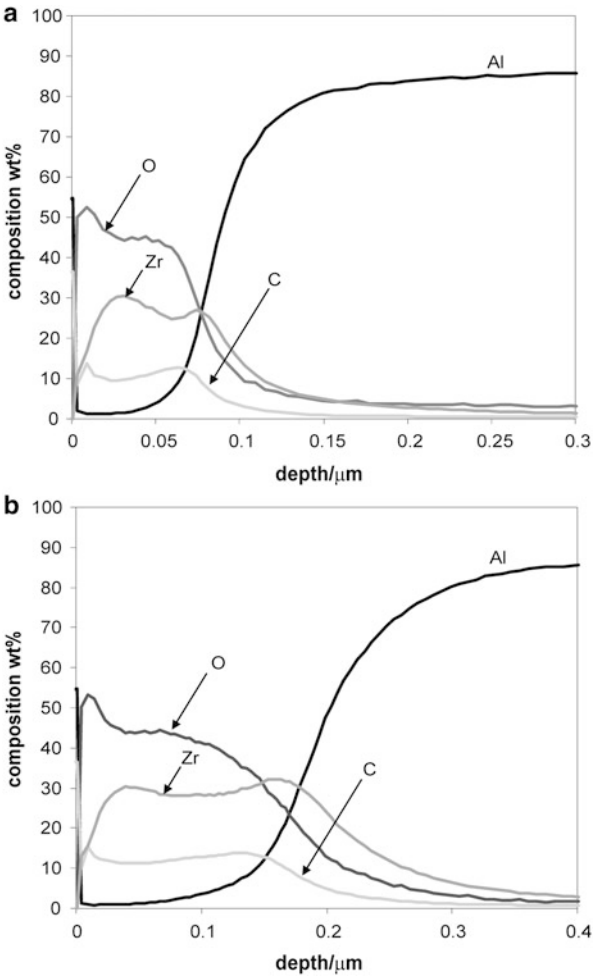

Fig. 4 GDOES composition profile of AA2024-T3 pretreated with a ZrO_2 sol-gel layer deposited by dipping technology using 0.1 M solution of metal–organic precursor. The profile in A is for a sample coated with one layer of ZrO_2; the profile in B is for a sample coated with three layers (Reprinted from Prog Org Coatings, 72, Andreatta F, Paussa L, Lanzutti A, Rosero Navarro NC, Aparicio M, Castro Y, et al., Development and industrial scale-up of ZrO2 coatings and hybrid organic-inorganic coatings used as pre-treatments before painting aluminium alloys, 3–14, Copyright (2011), with permission from Elsevier)

in the surrounding flat regions, where the pretreatment is uniform and without defects.

Figure 4 displays GDOES composition profiles acquired on AA2024-T3 pretreated with ZrO_2 sol-gel films. The profile in A is for a sample coated with one layer of ZrO_2 while the profile in B is for a sample coated with three layers. The GDOES profile in Fig. 4a evidences signals of Zr and O in the surface region, which are attributed to the ZrO_2 pretreatment on the alloy surface. The film thickness can be arbitrarily estimated by the intersection of the Al and Zr signals in the profile. This is about 80 nm for the ZrO_2 pretreatment consisting of a single layer produced with dipping technique. This estimation is rather rough due to the broad ZrO_2 film/substrate interface. However, it can be considered in line with film thickness observed in the TEM micrograph in Fig. 2. The GDOES profile in Fig. 4b relative to AA2024-T3 pretreated with three layers of ZrO_2 evidences similar trend to the

profile in Fig. 4a. Film thickness is about 180 nm for the pretreatment consisting of three layers. In general, it is observed that occurrence of defects in the films tends to become more probable increasing film thickness. Therefore, optimization of deposition procedures by dipping technology targeted the deposition of films with thickness in the range of 100 nm. This should be considered as optimum film thickness in order to obtain a nearly defect-free film morphology to provide good barrier properties to the sol-gel film.

Deposition of Pretreatments from Solution of Inorganic Precursor

Figure 5 shows a SEM micrograph of AA2024-T3 pretreated with a ZrO_2 sol-gel layer deposited from solution of inorganic precursor. The picture is taken at low magnification in order to show that film morphology is very similar to that obtained for deposition employing the metal–organic precursor. Indeed, the morphology of the pretreated sample evidences the surface structure obtained after surface preparation, as for the film produced with the metal–organic precursor solution. The SEM micrograph in Fig. 5 is relative to a sample for which the deposition by dipping technology was not still optimized. As a result, small cracks are visible at the locations of craters.

The GDOES profile in Fig. 6 exhibits Zr and O signals. The film thickness is about 180 nm for a film consisting of two layers. The film thickness for a single layer

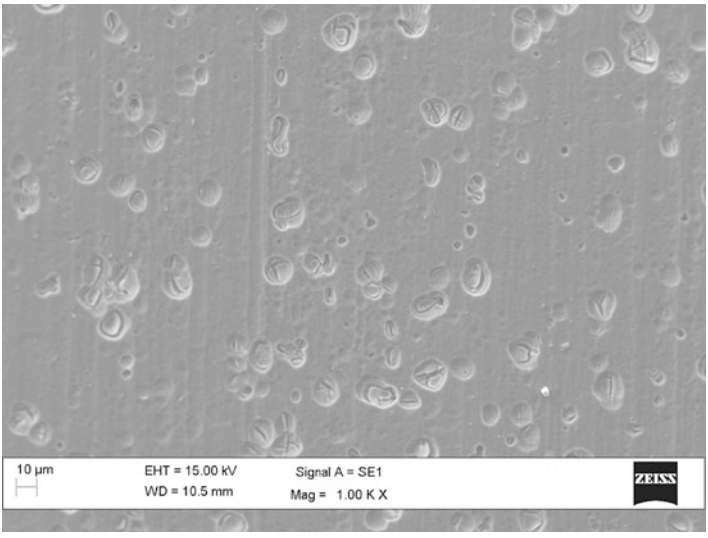

Fig. 5 SEM micrograph of AA2024-T3 pretreated with a ZrO_2 sol-gel layer deposited from 0.4 M solution of inorganic precursor (two layers) (Reprinted from Prog Org Coatings, 72, Andreatta F, Paussa L, Lanzutti A, Rosero Navarro NC, Aparicio M, Castro Y, et al., Development and industrial scale-up of ZrO2 coatings and hybrid organic-inorganic coatings used as pre-treatments before painting aluminium alloys, 3–14, Copyright (2011), with permission from Elsevier)

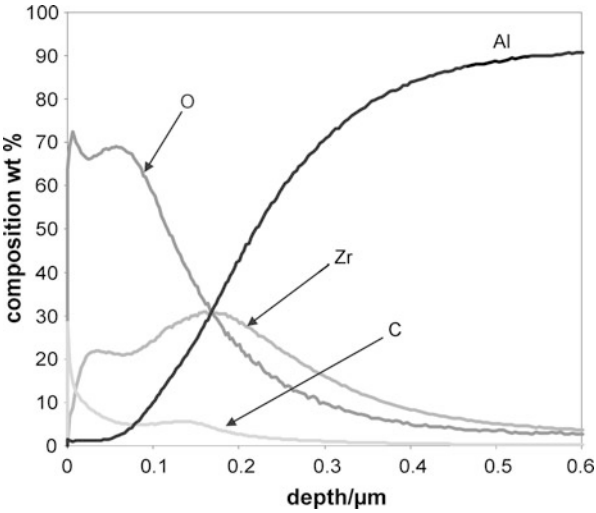

Fig. 6 GDOES composition profile of AA2024-T3 pretreated with a ZrO_2 sol-gel layer deposited employing 0.4 M solution of inorganic precursor (two layers) (Reprinted from Prog Org Coatings, 72, Andreatta F, Paussa L, Lanzutti A, Rosero Navarro NC, Aparicio M, Castro Y, et al., Development and industrial scale-up of ZrO2 coatings and hybrid organic-inorganic coatings used as pre-treatments before painting aluminium alloys, 3–14, Copyright (2011), with permission from Elsevier)

is about 70 nm (GDOES profile not shown here), in line with film thickness observed for the single-layer pretreatment obtained with a metal–organic precursor solution (Fig. 4a).

In the framework of research project MULTIPROTECT, it was decided to carry out the industrial scale-up by means of spraying technology for ZrO_2 pretreatments produced employing an inorganic precursor solution. This was performed by means of a robot-controlled air-pressure gun in a spraying cabin. The SEM micrograph in Fig. 7 shows the morphology of a sample produced according to an optimized procedure for deposition by spraying. The surface appears uniformly coated and without defects. This is an indication that the precursor solution employed for deposition by dipping can be also used for production of pretreatments using industrial equipment. The GDOES composition profile in Fig. 8 confirms the existence of a ZrO_2 film on the alloy surface, as can be seen by the trend of Zr and O signals. Film thickness is about 70 nm, which is in the same range than that of a single-layer pretreatment obtained by dipping.

Evaluation of Passive Corrosion Protection of Sol-Gel Films (Barrier Properties)

The morphology of sol-gel films shown in the previous sections clearly indicates that optimization of the deposition procedures can lead to the formation of nearly defect-free uniform films on AA2024-T3. Similar results were obtained for AA6060 (Andreatta et al. 2007; Paussa et al. 2012). Nevertheless, it should be considered that sol-gel films might contain different types of imperfections (film defects, cracks, nonuniform coverage), which can be related to surface preparation or sol-gel deposition procedures. These imperfections might affect the corrosion behavior of the

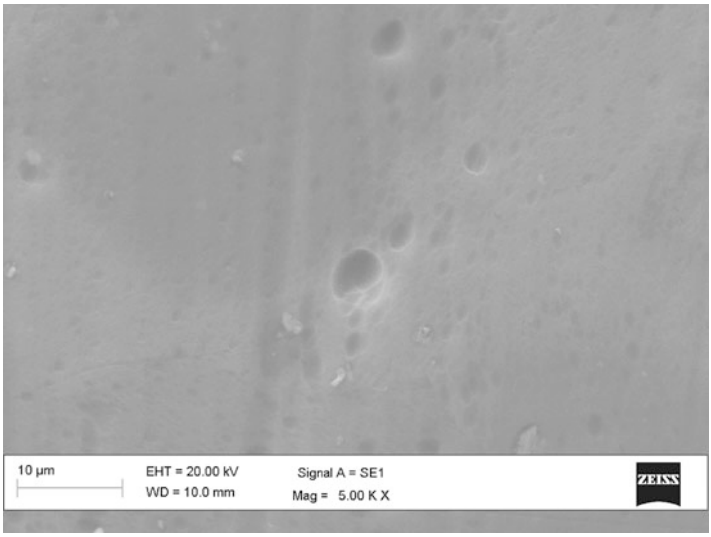

Fig. 7 SEM micrograph of AA2024-T3 coated with ZrO_2 sol-gel film deposited employing inorganic 0.4 M precursor solution by spraying technology (up-scaling using a robot-controlled air-pressure gun) (Reprinted from Prog Org Coatings, 72, Andreatta F, Paussa L, Lanzutti A, Rosero Navarro NC, Aparicio M, Castro Y, et al., Development and industrial scale-up of ZrO2 coatings and hybrid organic-inorganic coatings used as pre-treatments before painting aluminium alloys, 3–14, Copyright (2011), with permission from Elsevier)

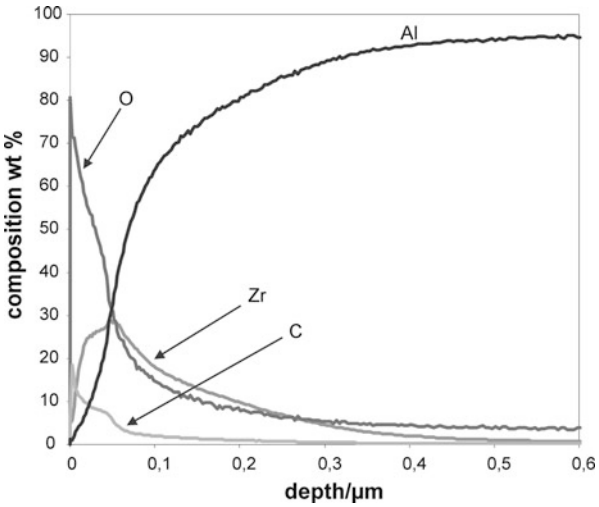

Fig. 8 GDOES composition profile of AA2024-T3 pretreated with a ZrO_2 sol-gel layer deposited from 0.4 M solution of inorganic precursor by spraying technology (up-scaling using a robot-controlled air-pressure gun) (Reprinted from Prog Org Coatings, 72, Andreatta F, Paussa L, Lanzutti A, Rosero Navarro NC, Aparicio M, Castro Y, et al., Development and industrial scale-up of ZrO2 coatings and hybrid organic-inorganic coatings used as pre-treatments before painting aluminium alloys, 3–14, Copyright (2011), with permission from Elsevier)

sol-gel films impairing their barrier effect. Therefore, it is very important to assess the barrier properties of sol-gel films in order to provide adequate corrosion protection to the metal substrate.

The electrochemical behavior of AA2024-T3 samples coated with ZrO_2 sol-gel films was investigated by means of potentiodynamic polarization in 0.05 M NaCl solution. Potentiodynamic polarization measurements were recorded using a Pt counter electrode and Ag/AgCl reference electrode. The area of the working electrode was 3.6 cm^2. The scan rate was 0.2 mV/s. The corrosion current density was estimated by means of extrapolation of the Tafel lines. Figure 9 shows potentiodynamic polarization curves for AA2024-T3 pretreated with optimized sol-gel coatings. The figure reports also the curves for the bare substrate and for chromate-conversion-coated AA2024, which was considered as reference for optimization of barrier properties. The curve for the ZrO_2 pretreatment applied by dipping in metal–organic precursor solution exhibits a corrosion current density of about 6×10^{-7} A cm^{-2}. This is almost two orders of magnitude lower than for bare AA2024 (3×10^{-5} A cm^{-2}). This indicates that the ZrO_2 pretreatment provides a barrier effect. This is further supported by the marked decrease of cathodic and anodic current density observed for the alloy coated with the ZrO_2 film deposited by dipping relative to the bare alloy. The anodic current density progressively increases above the corrosion potential at −0.52 V versus Ag/AgCl without displaying a clear passive range and breakdown potential. In contrast, the potentiodynamic

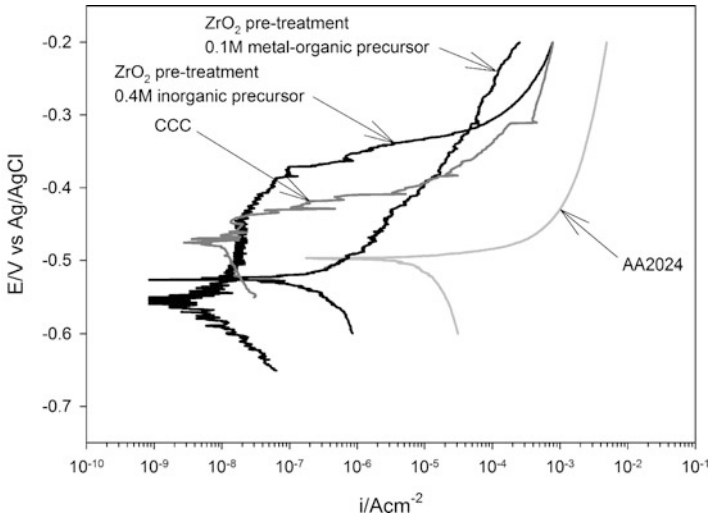

Fig. 9 Potentiodynamic polarization curves in 0.05 M NaCl solution for AA2024-T3 coated with ZrO_2 sol-gel films deposited employing metal–organic (0.1 M) and inorganic (0.4 M) precursor solutions. The curves for chromate-conversion-coated (CCC) AA2024-T3 and for bare substrate are also reported in the figure (Reprinted from Prog Org Coatings, 72, Andreatta F, Paussa L, Lanzutti A, Rosero Navarro NC, Aparicio M, Castro Y, et al., Development and industrial scale-up of ZrO2 coatings and hybrid organic-inorganic coatings used as pre-treatments before painting aluminium alloys, 3–14, Copyright (2011), with permission from Elsevier)

polarization curve for the ZrO_2 pretreatment applied by dipping in inorganic precursor solution displays a passive range extending between the corrosion potential at −0.55 V versus Ag/AgCl and the breakdown potential at –0.37 V versus Ag/AgCl. The corrosion current density is 1×10^{-8} A cm^{-2}. This clearly indicates that the pretreatment produced with the inorganic precursor solution further improves the barrier effect of the pretreatment obtained with the metal–organic precursor. Moreover, it can be seen in Fig. 9 that the ZrO_2 pretreatment produced with the inorganic precursor solution exhibits similar current density to the chromate conversion coating but more extended passive range. The barrier effect provided by sol-gel pretreatments is mainly due to the strong reduction of the area of active sites, as indicated by the marked reduction of corrosion current density for the samples coated with ZrO_2 films. Since the sol-gel film could be assumed inert in the aggressive electrolyte, the active sites are mainly film defects related to application of the film.

Figure 10 shows a potentiodynamic polarization curve for a sample coated with ZrO_2 pretreatment produced by spraying technology. In addition, a reference polarization curve produced by dipping technique using the same precursor solution is shown in the figure. Moreover, the figure shows the potentiodynamic polarization curve for a sample for which the deposition procedure by dipping was optimized in order to maximize barrier properties and the curve for the bare substrate. The

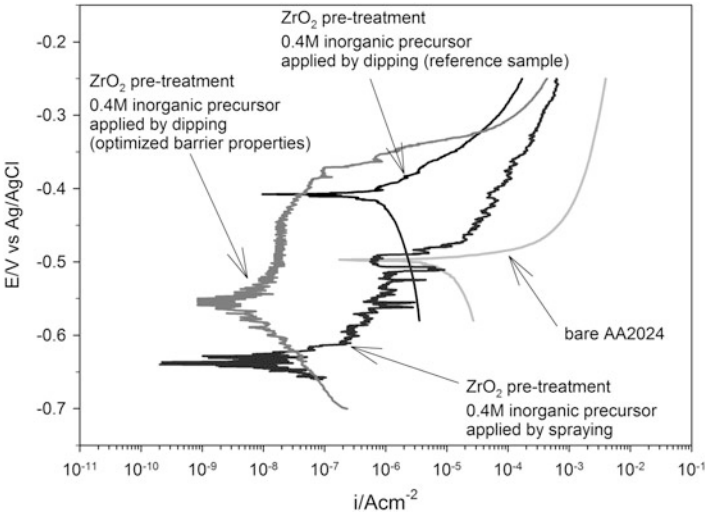

Fig. 10 Potentiodynamic polarization curves in 0.05 M NaCl solution for AA2024-T3 coated with ZrO_2 sol-gel films deposited employing inorganic 0.4 M precursor solution. The figure displays the curves relative to sample coated by spraying technology using a robot-controlled air-pressure gun and by dipping technique. The curve for the bare substrate is also reported in the figure (Reprinted from Prog Org Coatings, 72, Andreatta F, Paussa L, Lanzutti A, Rosero Navarro NC, Aparicio M, Castro Y, et al., Development and industrial scale-up of ZrO2 coatings and hybrid organic-inorganic coatings used as pre-treatments before painting aluminium alloys, 3–14, Copyright (2011), with permission from Elsevier)

potentiodynamic polarization curve for the ZrO_2 film deposited by spraying exhibits a corrosion current density of 3×10^{-8} A cm^{-2}. This is significantly lower than the corrosion current density of the reference pretreatment produced at laboratory scale by dipping technique (10^{-6} A cm^{-2}). However, the sample with optimized barrier properties (obtained by dipping) displays lower current density than the sample produced by spraying. Nevertheless, the very low corrosion current density measured for these two samples is an indication that the pretreatment provides an efficient barrier against corrosion. This is strengthened by the observation that the corrosion current density of the bare substrate is more than two orders of magnitude higher than for the sample coated with the pretreatment applied by spraying. The potentiodynamic polarization curve for ZrO_2 film deposited with a robot-controlled air-pressure gun exhibits an anodic current density that progressively increases above the open circuit potential and remains very low until a breakdown is observed at −0.48 V versus Ag/AgCl. The breakdown potential is 150 mV higher than the corrosion potential for this sample confirming the existence of a very good barrier against corrosion.

Comparison of the Barrier Properties of ZrO_2-Based Pretreatments with those of Cr- and Ti/Zr-Based Pretreatments

In order to consider ZrO_2 sol-gel films as an adequate alternative to commercial Cr- or Ti/Zr-based pretreatments, the barrier effect of sol-gel films should be better or at least at the same level than that of commercial pretreatments. Therefore, the electrochemical behavior of ZrO_2 pretreatments deposited on AA6060 was compared to that of chromatized and fluotitanated/fluozirconated AA6060 (Andreatta et al. 2007). The electrochemical behavior of the samples was investigated by means of cathodic and anodic potentiodynamic polarization measurements in diluted Harrison aqueous solution (0.05 wt% NaCl and 0.35 wt% $(NH_4)_2SO_4$). The counter electrode was a platinum wire (diameter 1.5 mm), and the reference electrode was Ag/AgCl for all measurements. The scan rate was 0.2 mV/s.

Figure 11 shows cathodic potentiodynamic polarization curves for as-received AA6060, chromatized AA6060, fluotitanated/fluozirconated AA6060, and sol-gel-pretreated AA6060 (3dip-250). The ZrO_2 sol-gel film on sample 3dip-250 was obtained by dip coating (3 dips) in a 0.1 M solution of $Zr(OBu^n)_4$ in anhydrous n-butanol, with a deposition procedure very similar to that described above for AA2024-T3. The thermal treatment was carried out at 250 °C for 4 min. Fluotitanated/fluozirconated AA6060 exhibits cathodic current density similar to as-received AA6060 over the entire cathodic polarization curve. In contrast, chromatized AA6060 exhibits a strong reduction of the cathodic current density indicating that chromate conversion layer inhibits cathodic reactions (Zhao et al. 1998; Ilevbare and Scully 2001). ZrO_2-pretreated AA6060 (3dip-250) exhibits a significant reduction of cathodic current density as compared to as-received AA6060. This decrease is quite similar to that observed for chromatized AA6060. The rather low cathodic current density observed in cathodic polarization for ZrO_2-

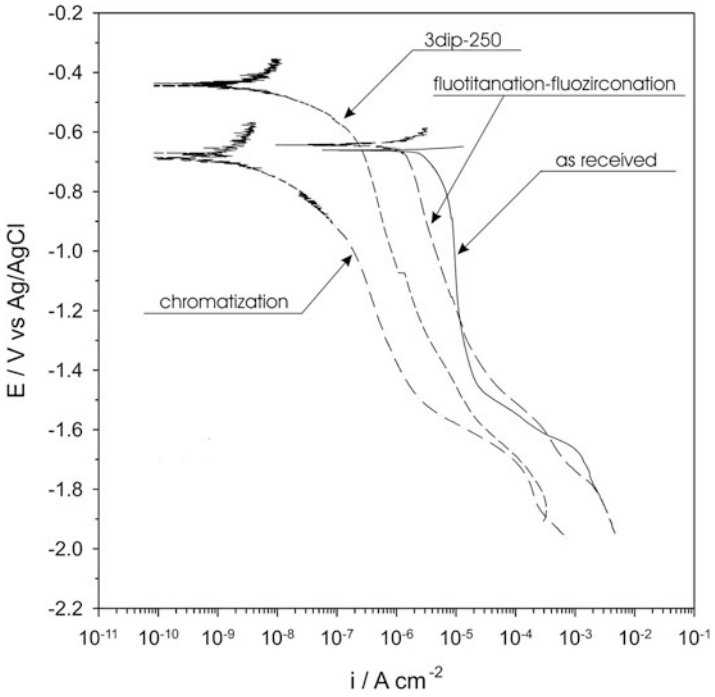

Fig. 11 Cathodic potentiodynamic polarization curves in diluted Harrison solution for as-received AA6060, chromatized AA6060, fluotitanated/fluozirconated AA6060, and ZrO_2-pretreated AA6060 (3dip-250) (Reprinted from Prog Org Coatings, 72, Andreatta F, Paussa L, Lanzutti A, Rosero Navarro NC, Aparicio M, Castro Y, et al., Development and industrial scale-up of ZrO2 coatings and hybrid organic-inorganic coatings used as pre-treatments before painting aluminium alloys, 3–14, Copyright (2011), with permission from Elsevier)

pretreated AA6060 (3dip-250) might indicate that the ZrO_2 layer inhibits the cathodic reaction similarly to chromatization. It is possible that the existence of an inert ceramic film on the surface might reduce the rate of oxygen transport to the alloy surface. Moreover, the ZrO_2 layer strongly reduces the area available for cathodic reactions, which are expected to take place only in the areas of the film containing defects.

As seen above for AA2024-T3, the anodic polarization curves could be strongly influenced by the existence of defects in the pretreatment. In particular, one can expect that the defects in the ZrO_2 layer are a preferential path for access of aggressive species to the alloy surface favoring localized attack. This behavior is shown in Figs. 12 and 13, which show, respectively, anodic polarization curves for pretreatments with good performance and for pretreatments containing defects. In both figures, anodic polarization curves are reported for as-received, chromatized, and ZrO_2-pretreated AA6060 (fluotitanated/fluozirconated AA6060 is shown only in Fig. 12). Figure 12 shows the anodic polarization curve for sample 3dip-250, while

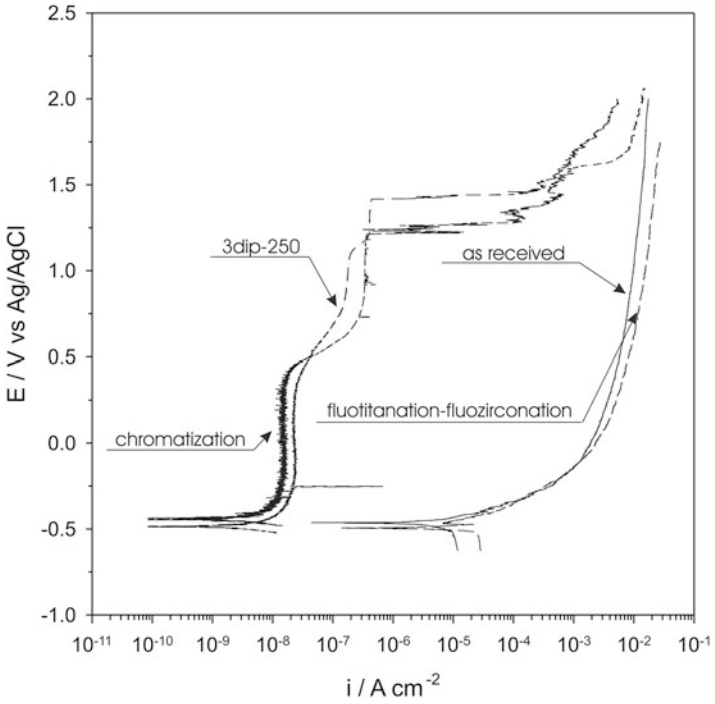

Fig. 12 Anodic potentiodynamic polarization curves in diluted Harrison solution for as-received AA6060, chromatized AA6060, fluotitanated/fluozirconated AA6060, and ZrO_2-pretreated AA6060 (3dip-250) (Reprinted from Electrochim Acta, 52, Andreatta F, Aldighieri P, Paussa L, Di Maggio R, Rossi S, Fedrizzi L, Electrochemical behaviour of ZrO2 sol-gel pre-treatments on AA6060 aluminium alloy, 7545–7555, Copyright (2007), with permission from Elsevier)

Fig. 13 displays the curve for sample 1dip-250 (sol-gel film obtained with only one dip in the precursor solution). As confirmed by SEM characterization (not shown here), the former sample presents a dense and continuous ZrO_2 layer on the alloy surface with almost no defects. In contrast, sample 1dip-250 exhibits several defects in the ZrO_2 film mainly in the form of cracks or small film portions detached from the substrate. The potentiodynamic polarization curve for fluotitanated/fluozirconated AA6060 does not show a passive range, and the breakdown of the passive film takes place at the open circuit potential, as for as-received AA6060. This indicates that the fluotitanation/fluozirconation pretreatment does not have significant barrier properties. In contrast, the anodic polarization curves for chromatized AA6060 and sample 3dip-250 (sol-gel-pretreated AA6060) exhibit an extended passive range characterized by very low anodic current density. This indicates that the deposited films are able to protect the substrate providing a good barrier against localized attack. In particular, ZrO_2-pretreated AA6060 show similar corrosion behavior to chromatized AA6060 in Fig. 12. This applies in the case of sol-gel pretreatment, which uniformly

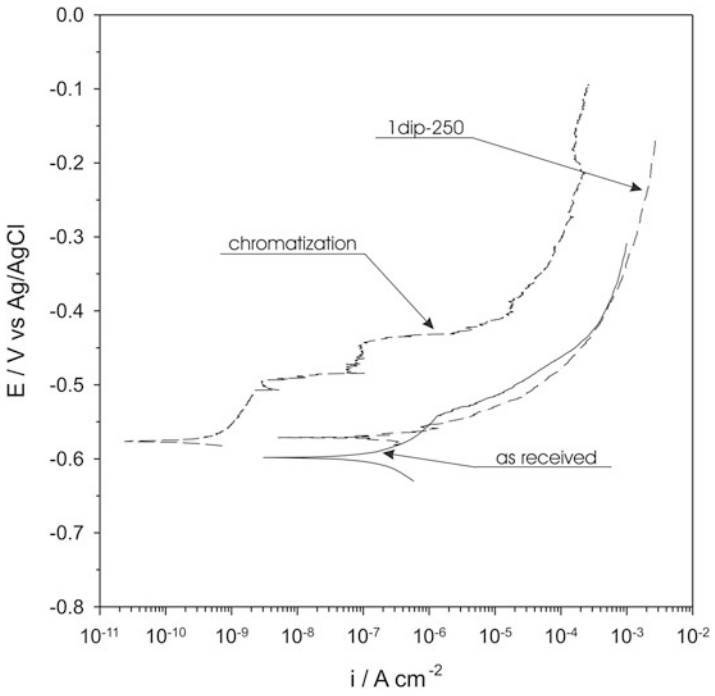

Fig. 13 Anodic potentiodynamic polarization curves in diluted Harrison solution for as-received AA6060, chromatized AA6060, and ZrO_2-pretreated AA6060 (1dip-250). These potentiodynamic polarization curves were performed on samples containing defects in the pretreatment (Reprinted from Electrochim Acta, 52, Andreatta F, Aldighieri P, Paussa L, Di Maggio R, Rossi S, Fedrizzi L, Electrochemical behaviour of ZrO2 sol-gel pre-treatments on AA6060 aluminium alloy, 7545–7555, Copyright (2007), with permission from Elsevier)

covers the surface and is not defected, as in the case of sample 3dip-250 in Fig. 12. The potentiodynamic polarization curve in Fig. 13 for sample 1dip-250 exhibits behavior similar to as-received AA6060 due to a large amount of defects present in the ZrO_2 layer. Also the curve for chromatized AA6060 (Fig. 13) displays a less extended passive range and higher anodic current density as compared to the curve for chromatized sample in Fig. 12. This behavior can be attributed to the existence of defects in the pretreatment and is related to a large variability of the protective properties of industrially produced chromate conversion coatings.

Figure 14 exhibits anodic potentiodynamic polarization curves for sol-gel pre-treatments on AA6060 obtained with different number of dips in the sol-gel bath. These curves exhibit a passive range with different extension (or no passive range as in the case of sample 1dip-250) and different anodic current density depending on the number of dips. This confirms that the properties of ZrO_2 pretreatments on AA6060 are strongly affected by process parameters and consequently by the presence of randomly distributed film flaws.

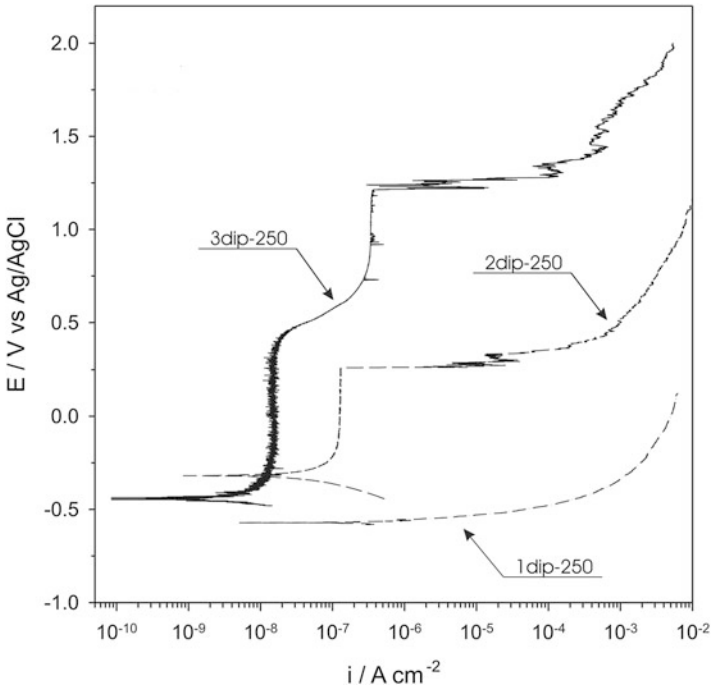

Fig. 14 Anodic potentiodynamic polarization curves in diluted Harrison solution for different ZrO2 pretreatments on AA6060 (1dip-250, 2dip-250, and 3dip-250) (Reprinted from Electrochim Acta, 52, Andreatta F, Aldighieri P, Paussa L, Di Maggio R, Rossi S, Fedrizzi L, Electrochemical behaviour of ZrO2 sol-gel pre-treatments on AA6060 aluminium alloy, 7545–7555, Copyright (2007), with permission from Elsevier)

Durability of ZrO_2 Sol-Gel Films

In the previous section, it has been shown that potentiodynamic polarization is a powerful tool for the evaluation of barrier properties of sol-gel coatings. A drawback of this electrochemical technique is that it is a destructive method. Indeed, the barrier properties are strongly impaired after the test since severe corrosion might be caused by sample polarization. Therefore, the assessment of long-term corrosion protection provided by sol-gel films is not possible by means of potentiodynamic polarization since it is not possible to follow how barrier properties change for long immersion times in an aggressive electrolyte. This information can be provided by open circuit potential measurements or by electrochemical impedance spectroscopy.

Open circuit potential and electrochemical impedance measurements were carried out for AA6060 in diluted Harrison aqueous solution. The counter electrode was a platinum wire (diameter 1.5 mm), and the reference electrode was Ag/AgCl for all measurements. A Pt mesh was used as counter electrode for impedance measurements. The measurements were carried out at room temperature in a standard electrochemical cell, and the area exposed was 14.8 cm^2 (80 ml electrolyte).

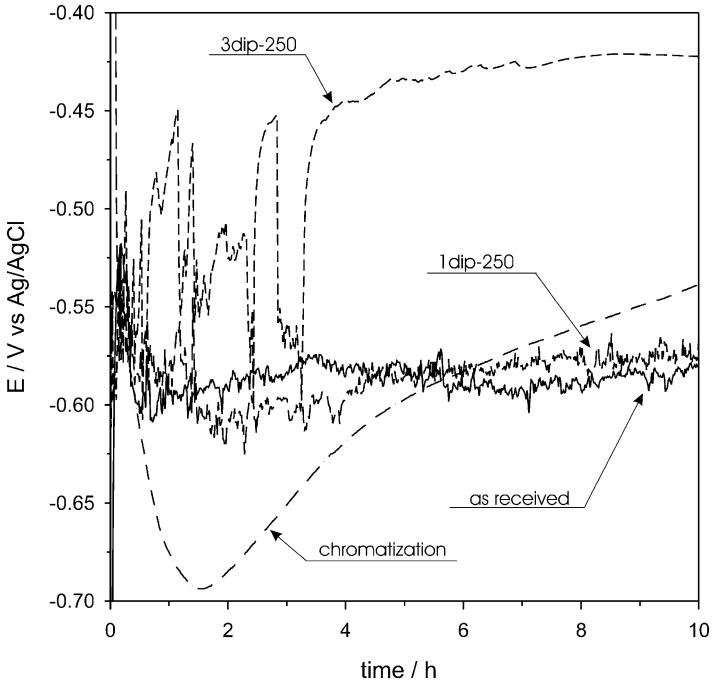

Fig. 15 Open circuit potential in diluted Harrison solution for as-received AA6060, chromatized AA6060, and ZrO_2-pretreated AA6060 (1dip-250 and 3dip-250) (Reprinted from Electrochim Acta, 52, Andreatta F, Aldighieri P, Paussa L, Di Maggio R, Rossi S, Fedrizzi L, Electrochemical behaviour of ZrO2 sol-gel pre-treatments on AA6060 aluminium alloy, 7545–7555, Copyright (2007), with permission from Elsevier)

Impedance measurements were carried out at open circuit potential with AC voltage amplitude of 10 mV and frequency range from 10 mHz to 100 kHz.

Figure 15 shows the open circuit potential for as-received, chromatized, and ZrO_2-pretreated AA6060 (1dip-250 and 3dip-250). The sample 1dip-250 shows similar open circuit potential to as-received AA6060. After an initial decrease due to surface activation, the open circuit potential becomes stable at a value of about −600 mV versus Ag/AgCl. The chromatized AA6060 exhibits an initial decrease of the open circuit potential during the first 2 h of immersion in solution. This is possibly related to activation of anodic reactions on the alloy surface and initiation of localized attack. Afterward the open circuit potential increases and becomes more noble than that of as-received AA6060 after 6 h of immersion. This trend continues even after an immersion time of 10 h. This ennoblement of the open circuit potential is most likely associated to repair of the conversion layer, which is a well-known phenomenon for chromate conversion coatings (Zhao et al. 1998; Xia et al. 2000; Ramsey and McCreery 1999). The open circuit potential of sample 3dip-250 shows a large scatter during the first 3 h of immersion and thereafter reaches a value more

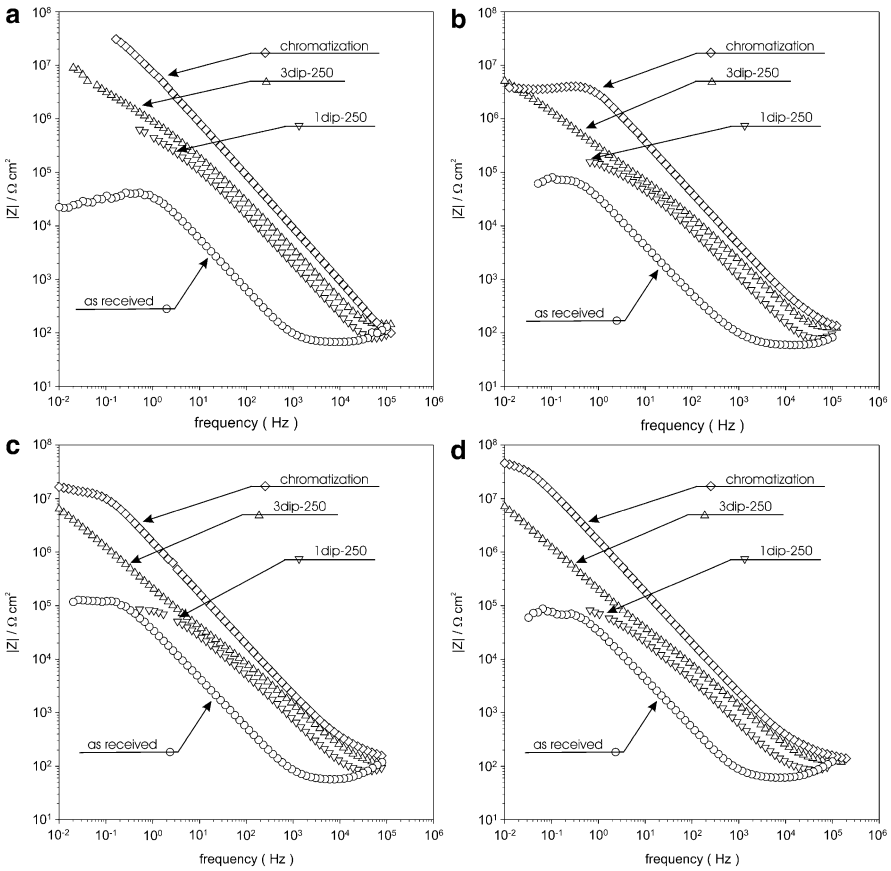

Fig. 16 Bode plots of the impedance modulus for different immersion times in diluted Harrison solution measured for as-received AA6060, chromatized AA6060, and ZrO_2-pretreated AA6060 (1dip-250 and 3dip-250): 0 h (**a**), 9 h (**b**), 24 h (**c**), and 48 h (**d**) (Reprinted from Electrochim Acta, 52, Andreatta F, Aldighieri P, Paussa L, Di Maggio R, Rossi S, Fedrizzi L, Electrochemical behaviour of ZrO2 sol-gel pre-treatments on AA6060 aluminium alloy, 7545–7555, Copyright (2007), with permission from Elsevier)

positive as compared to chromatized AA6060. The initial scatter shown by the open circuit potential is probably associated to the ceramic nature of the thin sol-gel film.

Since ZrO_2-pretreated AA6060 does not show a clear self-healing ability, it is very important to characterize the durability of this type of pretreatment by EIS measurements. Figure 16 shows Bode plots of the impedance modulus for different immersion times in diluted Harrison solution measured for as-received AA6060, chromatized AA6060, and sol-gel-pretreated AA6060 (1dip-250 and 3dip-250).

Figure 16a displays the Bode plot immediately after immersion in solution (0 h). Chromatized AA6060 exhibits the highest impedance module at low frequency

indicating that this pretreatment provides good barrier properties. Similarly, sample 3dip-250 shows a rather high impedance modulus at low frequency although about one order of magnitude lower than that of chromatized AA6060. Sample 1dip-250 exhibits similar behavior as sample 3dip-250 at high and intermediate frequencies. However, at low frequency, the measurement becomes unstable for this sample probably due to initiation of localized attack, which causes fluctuations of the open circuit potential. The existence of a protective oxide on the treated sample is also already visible in the behavior at high frequency as compared to that of as-received aluminum sample. After 9 h of immersion in solution (Fig. 16b), the impedance modulus at low frequency is in the same range for chromatized AA6060 and sample 3dip-250. Since the impedance modulus is rather high (4×10^6 Ωcm^2) for these samples, it can be stated that their barrier properties remain good after 9 h of immersion in diluted Harrison solution, although an impedance diagram with two time constants appears for the sol-gel-treated sample. Figure 16c shows the impedance spectra after an immersion time of 24 h. The impedance modulus at low frequency of sample 3dip-250 does not decrease with respect to the measurement for 9 h of immersion revealing good durability. Besides, the impedance modulus at low frequency slightly increases with respect to the value measured after 9 h of immersion for chromatized AA6060. This might be a first sign of dynamic recovery of the chromate oxide layer (self-healing). The impedance modulus at low frequency for sample 1dip-250 matches the value measured for as-received AA6060. This shows that this ZrO_2 pretreatment is not able to protect the substrate. The trend observed in Fig. 16c becomes more evident in Fig. 16d (48 h immersion time), where the impedance modulus at low frequency further increases for chromatized AA6060 and that for 3dip-250 sample remains rather constant.

An example of experimental and fitted data for chromatized AA6060 is shown in Fig. 17. This data was fitted with the equivalent circuit shown in Fig. 17a. The constant phase element CPE_{ox} and the resistor R_{ox} in Fig. 17a are used to model the nonideal capacitive behavior of the layer at the location of large defects like cracks (Goeminne et al. 1995; Campestrini et al. 2004). The double-layer capacitance is modeled with the constant phase element CPE_{dl}. R_{ct} and R_{el} are, respectively, the charge transfer resistance and the electrolyte resistance. The fit obtained with the equivalent circuit is very good both for the impedance module (Fig. 17b) and for the phase angle (Fig. 17c).

In order to fit the impedance data for ZrO_2 pretreatments on AA6060, the equivalent circuit in Fig. 18a was proposed (Andreatta et al. 2007). This circuit is based on the equivalent circuits reported in literature for chromate conversion coatings (Campestrini et al. 2004) and sol-gel films (Zheludkevich et al. 2006). The constant phase element CPE_{coat} describes the behavior of the intact ZrO_2 layer and the resistance R_p is related to the defect. The mesh describing the substrate (CPE_{dl} and R_{ct}) is in series with CPE_{ox} in the equivalent circuit in Fig. 18a, as seen for the circuit employed for fitting the data for chromate conversion layers. CPE_{ox} describes a network of electrolyte resistances and double-layer capacitors in the pores of the sol-gel layer, while R_{ox} is related to the barrier properties of the film. Based on the circuit shown in Fig. 18a, charge transfer processes take place on the

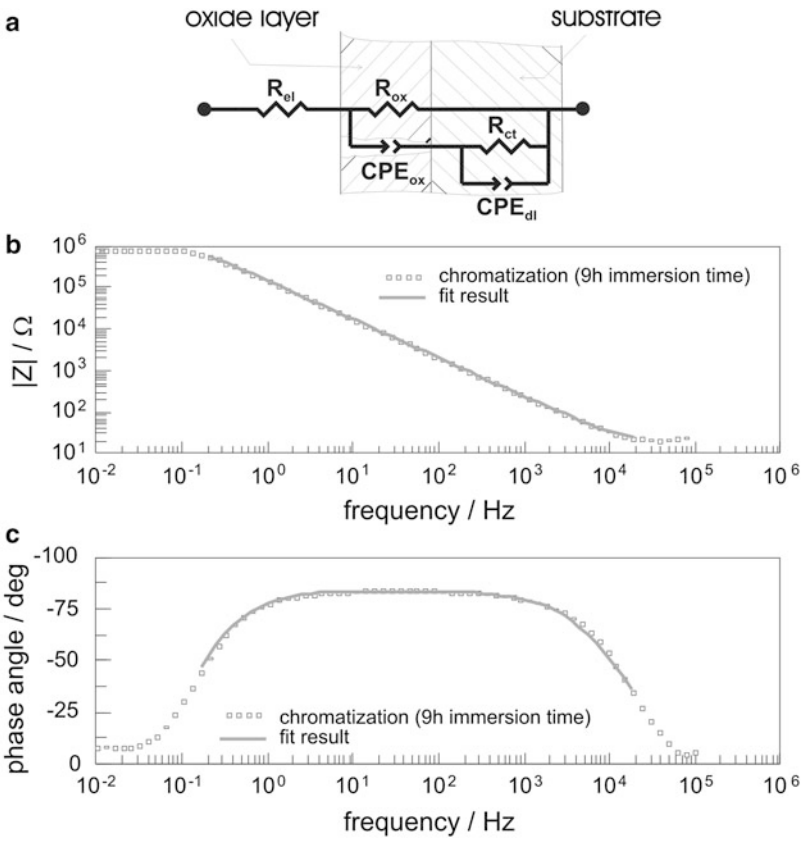

Fig. 17 Bode plots of the impedance modulus for different immersion times in diluted Harrison solution measured for as-received AA6060, chromatized AA6060, and ZrO_2-pretreated AA6060 (1dip-250 and 3dip-250): 0 h (**a**), 9 h (**b**), 24 h (**c**), and 48 h (**d**) (Reprinted from Electrochim Acta, 52, Andreatta F, Aldighieri P, Paussa L, Di Maggio R, Rossi S, Fedrizzi L, Electrochemical behaviour of ZrO2 sol-gel pre-treatments on AA6060 aluminium alloy, 7545–7555, Copyright (2007), with permission from Elsevier)

substrate, which is covered with a thin sol-gel layer. The parameter R_{ox} is affected by nanopores in this layer. Therefore, this is an important parameter of the equivalent circuit as far as corrosion protection is concerned.

Figure 19 shows the oxide resistance R_{ox} as a function of immersion time in diluted Harrison solution for chromatized and ZrO_2-pretreated AA6060 (sample 1dip-250 and 3dip-250). R_{ox} is calculated using the equivalent circuit in Figure 17a for chromatized AA6060 and the circuit in Fig. 18a for sol-gel-pretreated AA6060. R_{ox} for chromatized AA6060 exhibits an initial decrease during the first 10 h of immersion followed by an increase until a plateau region is reached between 72 and 150 h of immersion. R_{ox} for sample 3dip-250 exhibits an initial decrease of about one order of magnitude during the first 9 h of immersion followed by a limited

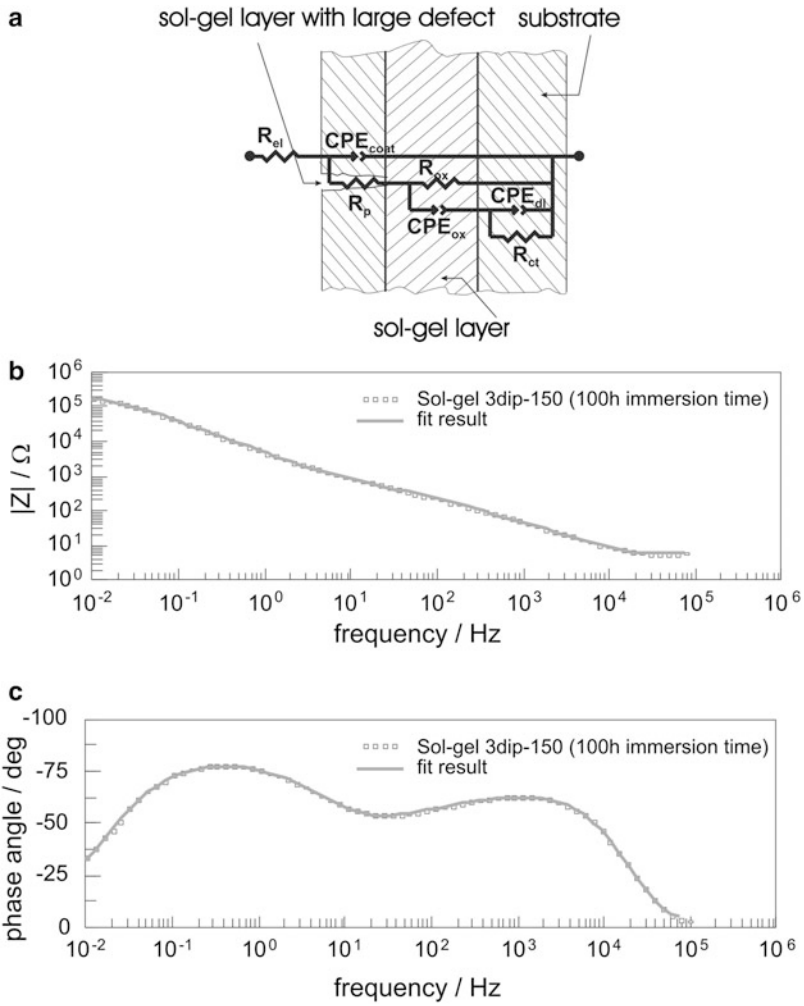

Fig. 18 Bode equivalent circuit (**a**) used to model impedance spectra reported as Bode plot for impedance modulus (**b**) and phase (**c**) for ZrO_2-pretreated AA6060 (3dip-150) (Reprinted from Electrochim Acta, 52, Andreatta F, Aldighieri P, Paussa L, Di Maggio R, Rossi S, Fedrizzi L, Electrochemical behaviour of ZrO2 sol-gel pre-treatments on AA6060 aluminium alloy, 7545–7555, Copyright (2007), with permission from Elsevier)

recovery. In contrast, sample 1dip-250 shows a marked decrease of R_{ox}. Moreover, R_{ox} for this sample is significantly lower than for sample 3dip-250 and chromatized AA6060 for the entire duration of the test. A decrease of R_{ox} was observed after more than 150 h immersion time for chromatized AA6060. The trend observed for R_{ox} of chromatized AA6060 indicates that the conversion layer is able to

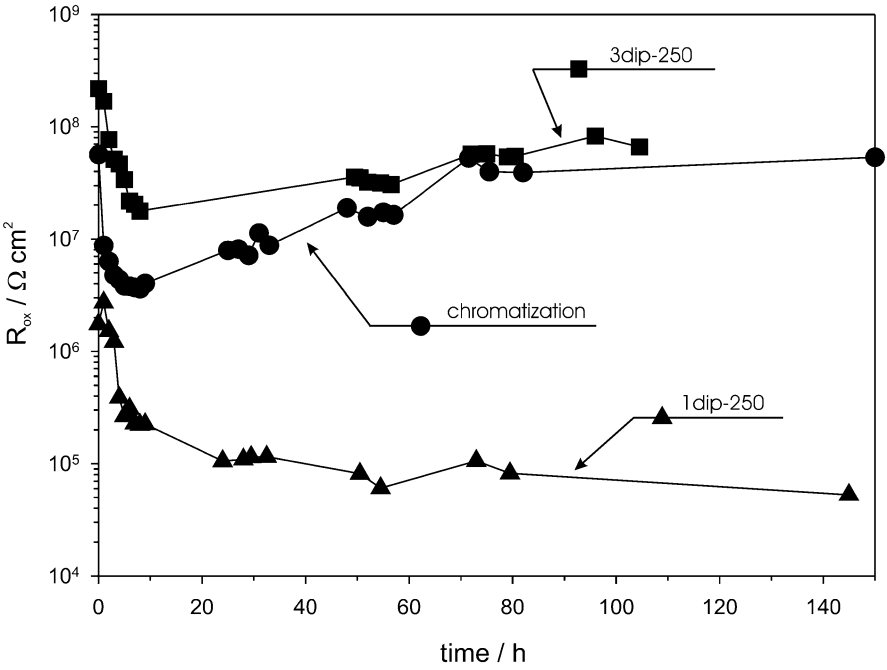

Fig. 19 Oxide resistance (R_{ox}) as a function of immersion time in diluted Harrison solution for chromatized AA6060 and for ZrO_2-pretreated AA6060 (1dip-250 and 3dip-250) (Reprinted from Electrochim Acta, 52, Andreatta F, Aldighieri P, Paussa L, Di Maggio R, Rossi S, Fedrizzi L, Electrochemical behaviour of ZrO2 sol-gel pre-treatments on AA6060 aluminium alloy, 7545–7555, Copyright (2007), with permission from Elsevier)

dynamically recover the barrier properties of the layer after an initial damage. This corresponds to the well-known self-healing ability of chromate conversion coatings. The behavior of ZrO_2-pretreated AA6060 is strongly dependent on the quality of the film formed on the alloy surface. Indeed, sample 1dip-250 exhibits a fast deterioration of the barrier properties that could be related to the existence of large defects in the ZrO_2 layer and to film detachment due to corrosion processes. In contrast, sample 3dip-250 exhibits barrier properties comparable to those of chromatized AA6060. This is related to the very limited number and small size of defects present in the ZrO_2 layer after a three-dip deposition. Besides, the 3dip-250 sample displays a limited recovery of the barrier properties after the initial deterioration during the first hours of immersion in solution. This limited recovery might be caused by the formation of corrosion products that could plug the defects or pores existing in the coating rather than by self-healing ability of the layer. This phenomenon is expected to be effective only for small defects in the ZrO_2 pretreatment, as in the case of sample 3dip-250.

Morphology and Electrochemical Behavior of Sol-Gel Films with Inhibitors

Deposition of Pretreatments Containing Corrosion Inhibitors

In general, self-healing is the self-recovery of the initial properties of a material after destructive interaction with the external environment, as seen for chromate conversion coatings in the previous section. In the context of pretreatment of aluminum alloys by sol-gel films, it can be considered that self-healing of a defect leads to complete recovery of the main coating functionality, which is corrosion protection. Hindering of corrosion activity in the defect by the coating itself can be considered a self-healing ability. This could be defined as active corrosion protection in more general terms. Introduction of inorganic or organic corrosion inhibitors in the coating is a possibility to develop active corrosion protection in sol-gel films. Different inhibitors could be considered for introduction in sol-gel coatings. Molybdenum is well known as a localized corrosion inhibitor when present in electrolyte as Mo VI (Twite and Bierwagen 1998; Magalhaes et al. 2004). Vanadium and manganese compounds are versatile corrosion inhibitors for aluminum alloys (Iannuzzi et al. 2007). Cerium and other rare-earth salts inhibit corrosion behavior of aluminum alloys in aqueous solution containing chlorides decreasing the cathodic reaction kinetics (Mansfeld et al. 1990; Hughes et al. 1995; Kendig and Buchheit 2003; Yasakau et al. 2006; Arnott et al. 1987; Zheludkevich et al. 2005a). Interesting results are reported for cerium salts added to sol-gel coatings on AA2024 aluminum alloy (Rosero-Navarro et al. 2008; Paussa et al. 2010b). Organic corrosion inhibitors have been studied alongside the inorganic ones as possible chromate replacements (Khramov et al. 2004; Yang and Van Ooij 2004). The inhibition effect of triazole and thiazole compounds has been investigated for aluminum alloys (Khramov et al. 2004; Zheludkevich et al. 2005b). Moreover, triazole and thiazole derivatives decrease the rate of the anodic reaction due to the formation of a protective film on the alloy. 8-Hydroxyquinoline inhibitor has been recently studied for aluminum alloys showing filming behavior due to absorption on the metal surface (Yasakau et al. 2008; Tang et al. 2006; Galio et al. 2010).

Although deposition of thin sol-gel layers leads to deposition of films with a very low number of defects, it is desirable to introduce corrosion inhibitors in the sol-gel films in order to improve corrosion resistance. This section presents different approaches for the introduction of corrosion inhibitors (cerium nitrate and 2-mercaptobenzothiazole) in ZrO_2 sol-gel films obtained using metal–organic and inorganic precursor solutions on AA2024-T3. In order to obtain sol-gel pretreatments doped with corrosion inhibitor, a dipping step in 0.3 M cerium nitrate solution was employed in the deposition procedure of the sol-gel pretreatments. The production of the sol-gel film containing 2-mercaptobenzothiazole was performed using a solution containing 6 g/l of the inhibitor. The contact time with the solution was about 30 s for each type of inhibitor. 2-Mercaptobenzothiazole could not be used for this system since the deposition of this inhibitor directly on the substrate impaired the adhesion of the sol-gel film. Figure 20 schematically shows the strategy followed

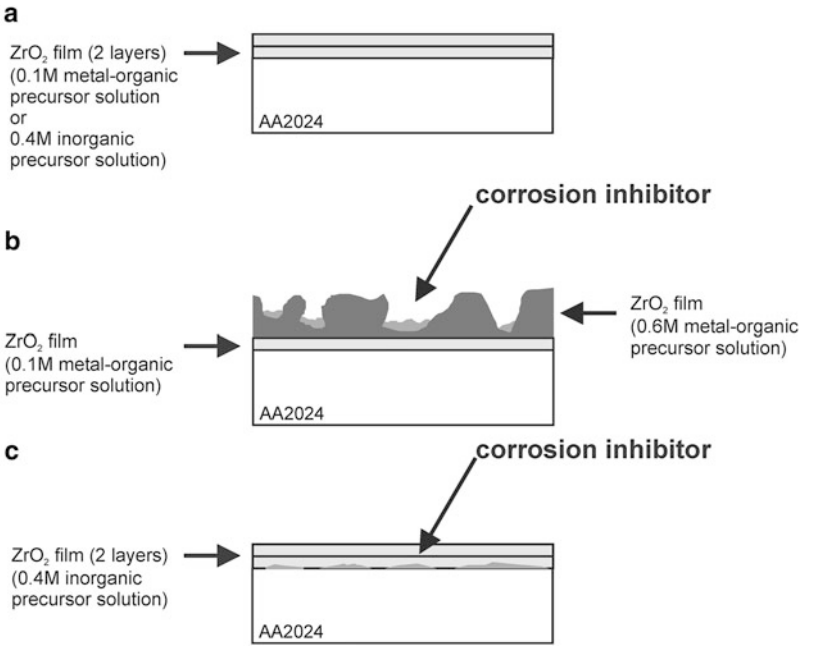

Fig. 20 Procedures followed for production of ZrO_2 pretreatment on AA2024 (**a**) and for introduction of corrosion inhibitor (cerium nitrate) in multilayer sol-gel coatings deposited using a solution of metal–organic (**b**) and inorganic precursor (**c**) (Reprinted from Prog Org Coatings, 69, Andreatta F, Paussa L, Aldighieri P, Lanzutti A, Raps D, Fedrizzi L, Corrosion behaviour of sol-gel treated and painted AA2024 aluminium alloy, 133–142, Copyright (2010a), with permission from Elsevier)

for the introduction of inhibitors in the sol-gel films by deposition of multilayer films.

The approach followed for the incorporation of corrosion inhibitors (cerium nitrate and 2-mercaptobenzothiazole) was dependent on the type of precursor solution employed for the deposition of the ZrO_2 sol-gel pretreatment. The deposition using a solution of metal–organic precursor offered the possibility of modifying the film structure by changing the precursor solution. Thin and compact films could be deposited using a 0.1 M precursor solution, while porous films were generated employing a 0.6 M solution. Since this porous structure might favor the incorporation of the inhibitor in the film, a multilayer structure was produced with an initial deposition carried out with 0.1 M metal–organic precursor solution followed by a deposition using a 0.6 M solution (Fig. 20b). Each deposition was followed by thermal treatment, as described above for the pretreatment without inhibitor. The inhibitor was introduced in the multilayer sol-gel structure by means of a final dip in the inhibitor solution in order to favor impregnation of the porous structure with the inhibitor (Fig. 20b). The production of sol-gel films containing cerium nitrate starting from inorganic precursor solution was carried out with an initial dip in

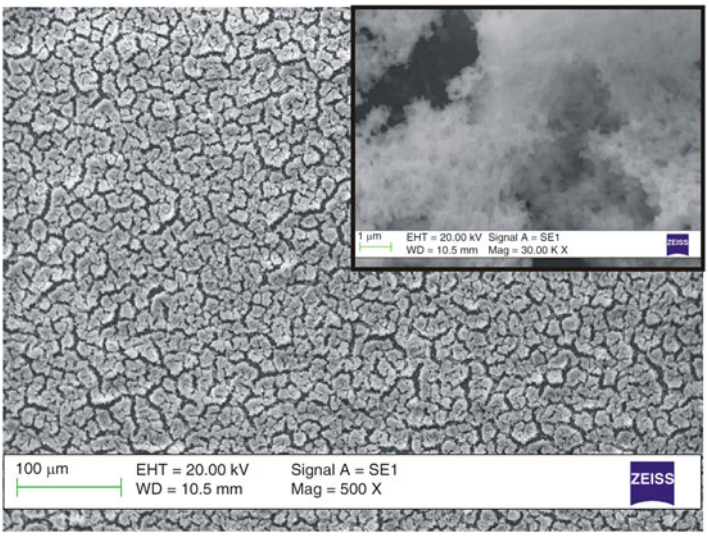

Fig. 21 SEM micrograph of AA2024 coated with a multilayer sol-gel film containing cerium nitrate. The sol-gel film was deposited using a metal–organic precursor solution with 0.1 M concentration for the first layer and 0.6 M for the second one (Reprinted from Prog Org Coatings, 69, Andreatta F, Paussa L, Aldighieri P, Lanzutti A, Raps D, Fedrizzi L, Corrosion behaviour of sol-gel treated and painted AA2024 aluminium alloy, 133–142, Copyright (2010a), with permission from Elsevier)

$0.3MCe(NO_3)_3$ solution followed by deposition of two layers of ZrO_2 using the 0.4 M $ZrO(NO_3)_2$ water-based solution (Fig. 20c), as described above for the production of non-inhibited films (Fig. 20a). This was necessary because it was not possible to produce a porous structure employing the inorganic precursor solution.

Figure 21 shows the morphology of a multilayer pretreatment consisting of a first layer produced with 0.1 M metal–organic precursor solution and a second layer deposited with 0.6 M solution. This second layer appears very porous even in a nanometric scale, as it is visible in the SEM micrograph in the insert in Fig. 21. The morphology resulting from deposition with 0.6 M solution favors storage of corrosion inhibitors in the porous structure of the sol-gel film. The introduction of cerium species in the multilayer structure was performed with a final dip in a solution of cerium nitrate, as described in Fig. 20b.

The GDOES semiquantitative composition profile in Fig. 22 evidences the Ce signal in the ZrO_2 multilayer structure suggesting that the inhibitor solution deeply penetrates in the spongy ZrO_2 film. The trend of the Ce signal in the insert of Fig. 22 suggests that there is a higher concentration of Ce species at the interface between sol-gel layer and AA2024 substrate than on the outer layer of the coating. A possible explanation for this behavior is that cerium species tend to accumulate at the bottom of pores obtained in the sol-gel film by deposition from a 0.6 M precursor solution according to the preparation procedure in Fig. 20b. In addition, film thickness is

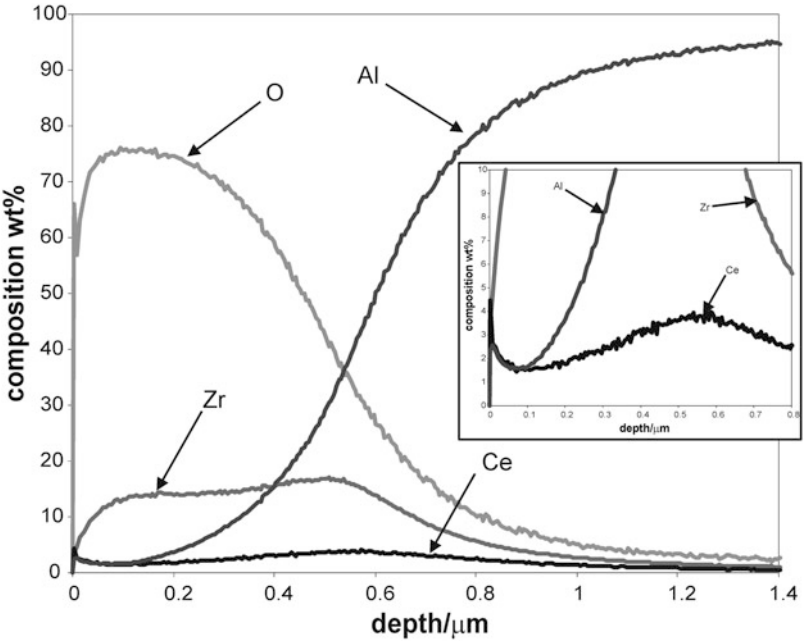

Fig. 22 GDOES semiquantitative composition profile of AA2024 coated with a multilayer sol-gel film containing cerium nitrate. The sol-gel film was deposited using a metal–organic precursor solution with 0.1 M concentration for the first layer and 0.6 M for the second one (Reprinted from Prog Org Coatings, 69, Andreatta F, Paussa L, Aldighieri P, Lanzutti A, Raps D, Fedrizzi L, Corrosion behaviour of sol-gel treated and painted AA2024 aluminium alloy, 133–142, Copyright (2010a), with permission from Elsevier)

about 550 nm, which is significantly higher as compared to the similar pretreatment obtained with 0.1 M precursor solution (Fig. 4). Thus, the deposition of the porous layer with 0.6 M metal–organic solution leads to a marked increase in film thickness. This is most likely associated to the higher viscosity of the 0.6 M solution relative to the 0.1 M one resulting in the typical morphology visible in Fig. 21. This structure might enhance mechanical interlocking of paints with the pretreatment promoting paint adhesion. The adhesion of the porous layer obtained with 0.6 M precursor solution to the underlying layer produced with 0.1 M is very good, and no detachments between different layers are generally observed in multilayer structures. In addition, the adhesion of the first layer to the substrate remains good, as seen for the pretreatments without inhibitors.

Figure 23 shows the morphology of a ZrO_2 pretreatment containing cerium species produced with a 0.4 M inorganic precursor solution according to the procedure shown in Fig. 20c. The film morphology is very similar to that discussed in Fig. 5 for the film without inhibitor.

The thickness of the multilayer structure is about 250 nm, as can be seen in the GDOES profile in Fig. 24. The profile reveals the Ce signal in the pretreatment

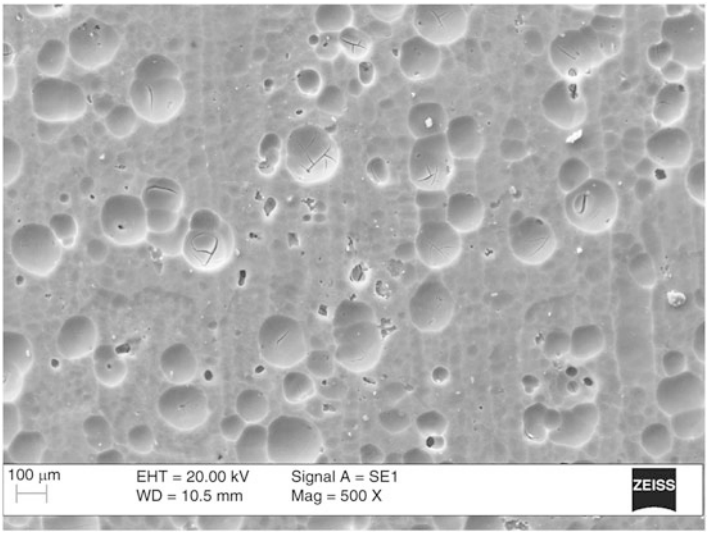

Fig. 23 SEM micrograph of AA2024 coated with a multilayer sol-gel film containing cerium nitrate. The sol-gel film consists of two layers produced with a 0.4 M inorganic precursor solution (Reprinted from Prog Org Coatings, 69, Andreatta F, Paussa L, Aldighieri P, Lanzutti A, Raps D, Fedrizzi L, Corrosion behaviour of sol-gel treated and painted AA2024 aluminium alloy, 133–142, Copyright (2010a), with permission from Elsevier)

indicating that Ce species could be successfully introduced in the sol-gel film. Moreover, the trend of the Ce signal in the insert of Fig. 24 displays a higher concentration of Ce species at the interface between sol-gel layer and AA2024 substrate. This can be an important advantage in terms of corrosion protection since the active Ce species are in direct contact with the substrate and might have an inhibition effect on corrosion reactions that might occur in aggressive electrolytes.

Barrier Properties of Sol-Gel Films Containing Corrosion Inhibitors

Figure 25 displays potentiodynamic polarization curves for ZrO_2 pretreatments containing corrosion inhibitors (2-mercaptobenzothiazole and cerium nitrate). In addition, the figure displays the potentiodynamic polarization curves for an undoped ZrO_2 pretreatment with optimized barrier properties and for the bare substrate. The curve for the ZrO_2 pretreatment doped with 2-mercaptobenzothiazole (applied by spraying) evidences a passive range (about 200 mV) and breakdown potential at −0.37 V versus Ag/AgCl. Moreover, it displays a marked reduction of cathodic and anodic current density with respect to the undoped pretreatment. In particular, the addition of 2-mercaptobenzothiazole promotes the reduction of cathodic current density since this inhibitor is known to be an efficient inhibitor of cathodic reactions. The combination of an efficient barrier layer and inhibition due to

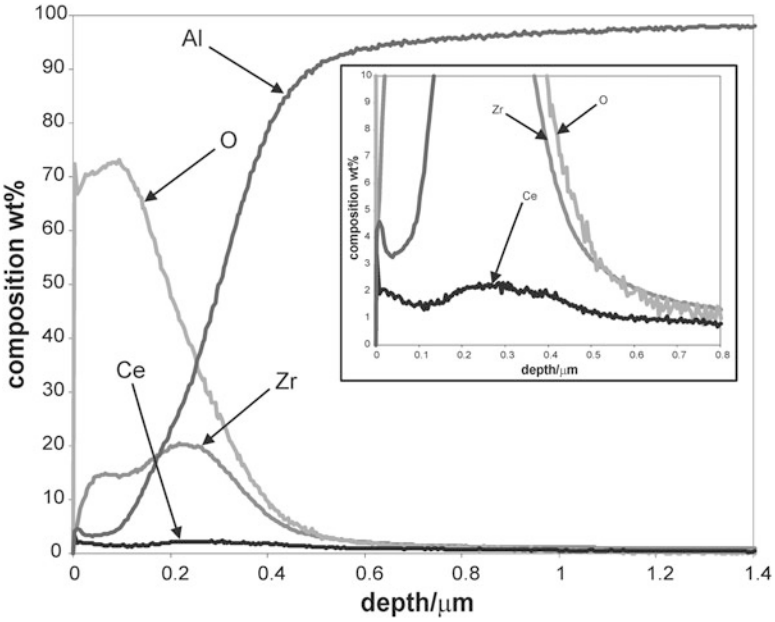

Fig. 24 GDOES semiquantitative composition profile of AA2024 coated with a multilayer sol-gel film containing cerium nitrate. The sol-gel film consists of two layers produced with a 0.4 M inorganic precursor solution. The insert in the figure evidences the trend of Ce signal in the sol-gel coating (Reprinted from Prog Org Coatings, 69, Andreatta F, Paussa L, Aldighieri P, Lanzutti A, Raps D, Fedrizzi L, Corrosion behaviour of sol-gel treated and painted AA2024 aluminium alloy, 133–142, Copyright (2010a), with permission from Elsevier)

2-mercaptobenzothiazole leads to good corrosion protection of the substrate during potentiodynamic polarization. The potentiodynamic polarization curve for ZrO_2 pretreatment doped with cerium nitrate exhibits cathodic and anodic current density similar to that of the sol-gel pretreatment without inhibitor. The same behavior is observed for the corrosion current density. In this case, the inhibitor does not significantly improve the corrosion resistance of the system. This behavior could be related to the short time employed for the immersion of the samples in the solution containing cerium nitrate. Nevertheless, the introduction of cerium nitrate in sol-gel films was considered an important issue in the development phase of ZrO_2 pretreatments since this inhibitor might provide self-healing ability to the corrosion protection system.

Figure 26 reports the potentiodynamic polarization curve for a ZrO_2 pretreatment produced with inorganic precursor solution and containing cerium nitrate. The figure shows also the curves for the ZrO_2 film obtained using inorganic precursor without inhibitor (optimized barrier properties) and for the bare substrate. Although the corrosion behavior of the ZrO_2 pretreatment containing cerium nitrate is not as good as that of the pretreatment without inhibitor and optimized barrier properties, the potentiodynamic polarization curve for the pretreatment containing cerium

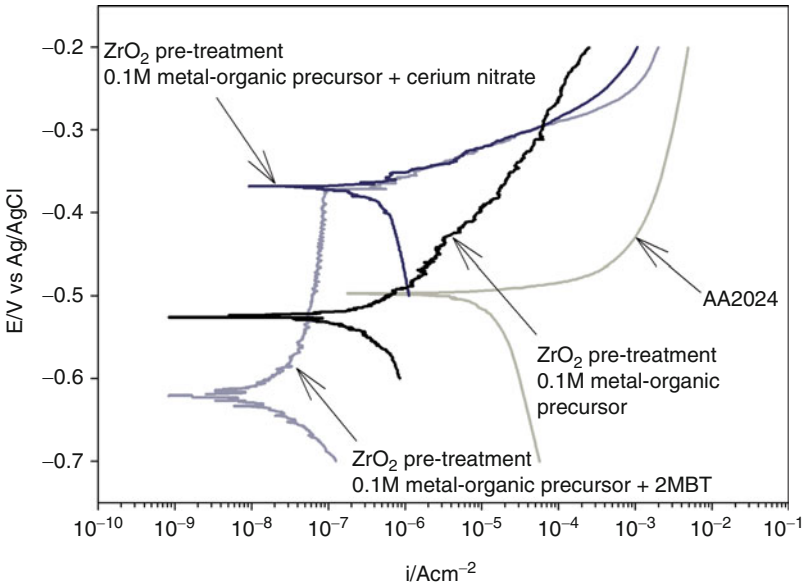

Fig. 25 Potentiodynamic polarization curves in 0.05 M NaCl solution for AA2024-T3 coated with ZrO_2 sol-gel films deposited employing metal–organic 0.1 M precursor solution and containing corrosion inhibitors (2-mercaptobenzothiazole and cerium nitrate). The curves for the ZrO_2 film obtained using metal–organic precursor without inhibitors and for bare substrate are also reported in the figure (Reprinted from Prog Org Coatings, 72, Andreatta F, Paussa L, Lanzutti A, Rosero Navarro NC, Aparicio M, Castro Y, et al., Development and industrial scale-up of ZrO2 coatings and hybrid organic-inorganic coatings used as pre-treatments before painting aluminium alloys, 3–14, Copyright (2011), with permission from Elsevier)

nitrate displays low cathodic and anodic current density. Moreover, the corrosion current density is 10^{-7} A cm^{-2} for the pretreatment containing the inhibitor, confirming the barrier effect of the pretreatment. The inhibition effect of cerium species could not be clearly identified in potentiodynamic polarization tests carried out on sol-gel films produced using inorganic precursor and containing cerium nitrate.

Hybrid Sol-Gel Films Containing Corrosion Inhibitors

Another approach for the introduction of corrosion inhibitors in sol-gel films is the production of hybrid sol-gel films by dip coating technique (Rosero-Navarro et al. 2010; Andreatta et al. 2011). The hybrid coating is a methacrylate silane-based hybrid film containing SiO_2 nanoparticles. The structure of the hybrid coating was composed of three layers. The intermediate layer is doped with cerium, whereas the other layers do not contain cerium. The layer doped with cerium nitrate is located

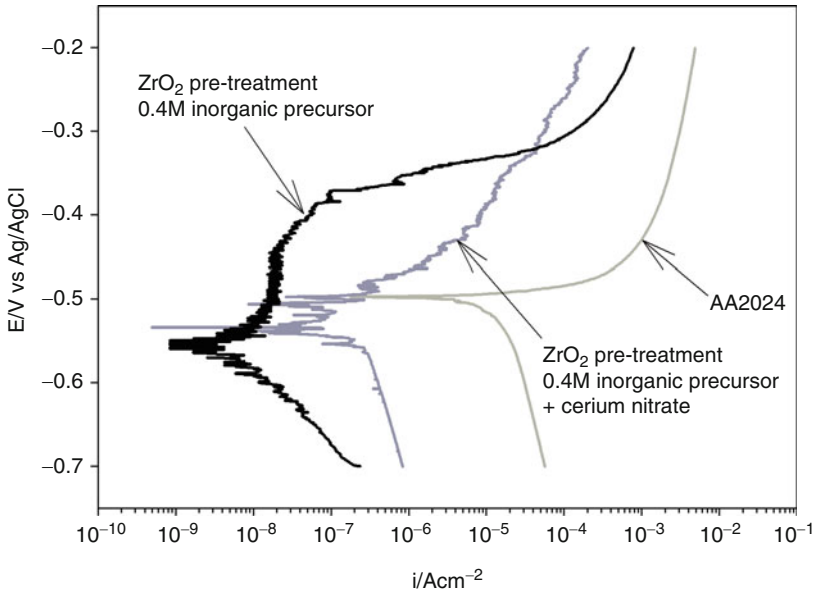

Fig. 26 Potentiodynamic polarization curves in 0.05 M NaCl solution for AA2024-T3 coated with ZrO_2 sol-gel films deposited employing inorganic 0.4 M precursor solution and containing corrosion inhibitor (cerium nitrate). The curves for the ZrO_2 film obtained using inorganic precursor without inhibitor and for bare substrate are also reported in the figure (Reprinted from Prog Org Coatings, 72, Andreatta F, Paussa L, Lanzutti A, Rosero Navarro NC, Aparicio M, Castro Y, et al., Development and industrial scale-up of ZrO2 coatings and hybrid organic-inorganic coatings used as pre-treatments before painting aluminium alloys, 3–14, Copyright (2011), with permission from Elsevier)

in the middle of the coating system to prevent a premature cerium lixiviation to the electrolyte and to avoid a poor wettability on the metal substrate. The hybrid organic–inorganic coating can be employed either as a pretreatment for successive deposition of primer and topcoat or as a complete corrosion protection system without the need of the organic coating.

Figure 27a reports a scheme of the structure of hybrid coatings. The GDOES profile in Fig. 29b shows the wt% composition as a function of the sputtering time. The Si and O signals clearly reveal the three layers constituting the hybrid film. The intermediate layer is clearly identified by the Ce signal. The interface between the hybrid organic–inorganic coating is located at about 120 s sputtering time, which corresponds to a film thickness of about 8 μm. Therefore, hybrid films are much thicker than ZrO_2 sol-gel pretreatments considered above with thickness in the range of 100 nm.

Figure 28a reports the Nyquist plot for the hybrid organic–inorganic film containing cerium nitrate as a function of immersion time. The Nyquist plot recorded immediately after immersion (0 h) exhibits at high frequency a semicircle that can be

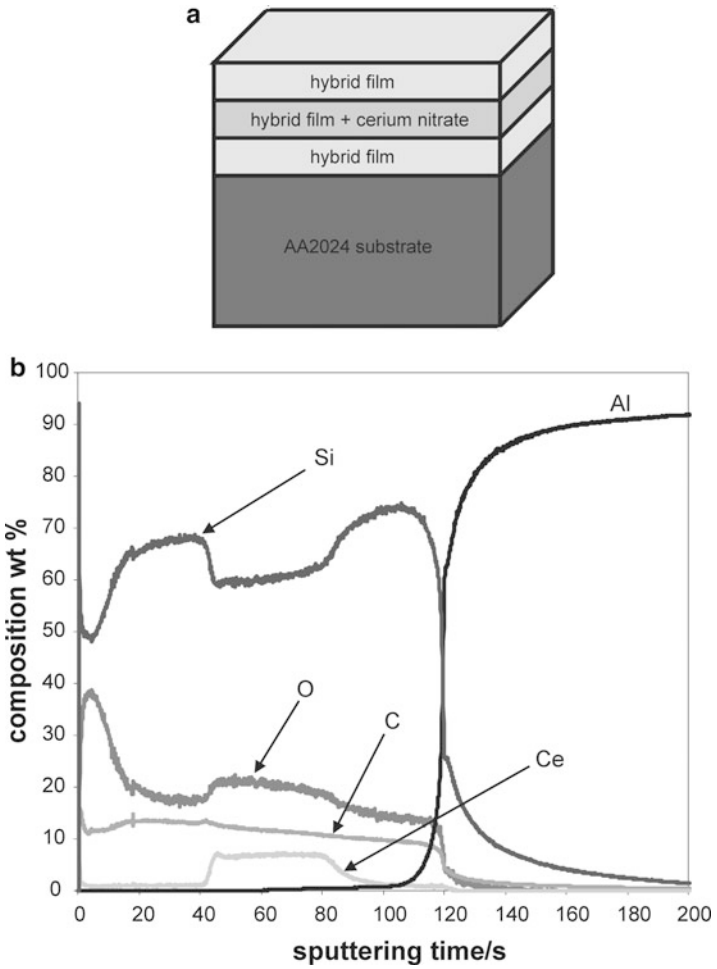

Fig. 27 Scheme of the hybrid film (**a**) and GDOES composition profile (wt% weight composition vs. sputtering time) for AA2024-T3 coated with a hybrid sol-gel coating inhibited with cerium nitrate (**b**) (Reprinted from Prog Org Coatings, 72, Andreatta F, Paussa L, Lanzutti A, Rosero Navarro NC, Aparicio M, Castro Y, et al., Development and industrial scale-up of ZrO2 coatings and hybrid organic-inorganic coatings used as pre-treatments before painting aluminium alloys, 3–14, Copyright (2011), with permission from Elsevier)

attributed to the electrochemical contribution of the hybrid coating. The contribution of faradic reactions at the metal substrate can be identified at low frequency. The diameter of the semicircle at high frequency progressively decreases as a function of immersion time indicating that the hybrid coating undergoes degradation of barrier properties in the electrolyte. This is evident for the impedance plot recorded after 196 h of immersion. In order to evidence the inhibition related to the introduction of cerium nitrate in the hybrid organic–inorganic pretreatment, the charge transfer

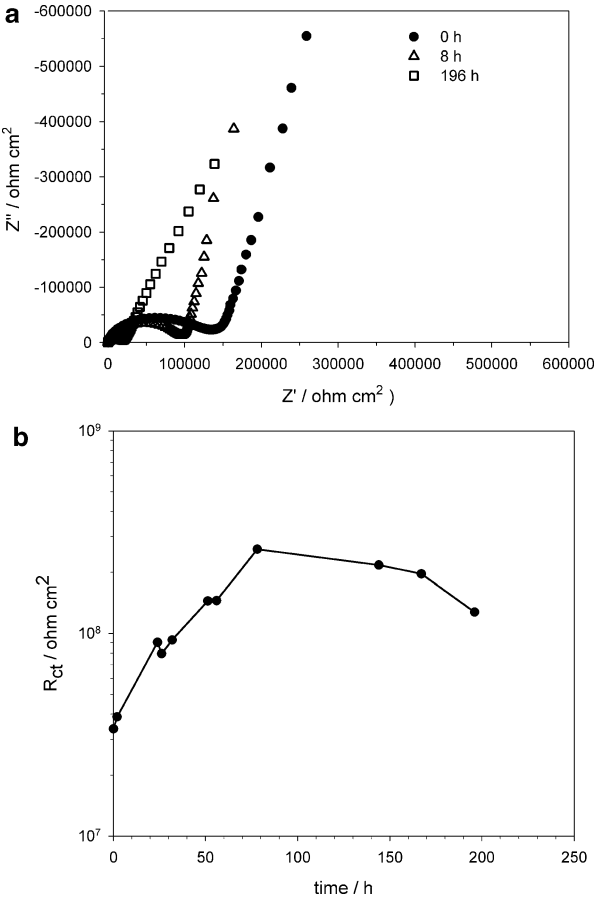

Fig. 28 Nyquist plots of electrochemical impedance recorded in 0.05 M NaCl solution for AA2024-T3 coated with a hybrid sol-gel coating inhibited with cerium nitrate (**a**) and charge transfer resistance (Rct) as a function of immersion time (**b**) (Reprinted from Prog Org Coatings, 72, Andreatta F, Paussa L, Lanzutti A, Rosero Navarro NC, Aparicio M, Castro Y, et al., Development and industrial scale-up of ZrO2 coatings and hybrid organic-inorganic coatings used as pre-treatments before painting aluminium alloys, 3–14, Copyright (2011), with permission from Elsevier)

resistance (R_{ct}) of the system was calculated employing an equivalent circuit (Rosero-Navarro et al. 2010). Figure 28b shows that R_{ct} progressively increases during 70 h of immersion in the electrolyte and start to decrease only for longer immersion times. This behavior is observed only in the case of inhibited hybrid coatings, while it was not found in the same system without cerium nitrate. The progressive increase of R_{ct} as a function of immersion time clearly indicates that there is a reduction of the corrosion rate of the substrate. Since the barrier effect is very limited for the hybrid organic–inorganic film, the reduction of corrosion rate is most likely due to the inhibition effect of cerium nitrate. It is expected that cerium species might precipitate at the coating/substrate interface reducing active areas on the substrate. It is proven that this behavior is associated to migration of cerium species from the hybrid coating to the coating/substrate interface, as discussed in detail in other papers (Rosero-Navarro et al. 2010; Paussa et al. 2012).

Evaluation of Adhesion of an Organic Primer and Topcoat on Sol-Gel Films by Means of Electrochemical Methods

Since ZrO_2 sol-gel films considered in this chapter are designed as pretreatments, evaluation of paint adhesion of organic primers and topcoats is an important issue in the development phase of sol-gel pretreatments. In order to test the adhesion properties of ZrO_2 films deposited with sol-gel technique, AA6060 covered with ZrO_2 films and fluotitanated/fluozirconated and chromatized AA6060 samples were painted with polyester type coating (the thickness of the topcoat was 20 μm for all samples). Coated samples underwent thermal cycles in 0.05 wt% NaCl solution (the area exposed was 3.6 cm^2). Each thermal cycle consisted of heating the samples at 80 °C (above the glass transition temperature of the paint), permanence at this temperature for 6 h, and cooling and permanence at room temperature for 18 h. Impedance measurements were performed at the end of each cycle. The impedance results were fitted by Zview Software, in order to obtain the admittance modulus of the related constant phase element of the coating. This provides information about the adhesion behavior of the coating (Fedrizzi et al. 2006).

Figure 29 shows the Bode plot for the impedance modulus measured at the end of each thermal aging cycle for chromatized and painted AA6060. Thermal cycle number 0 is an impedance measurement performed in solution before performing the first thermal cycle. The impedance modulus is rather high (about 10^{11} Ωcm^2) for 26 thermal cycles, while at the 27th thermal cycle, there is a decrease of the impedance modulus. Figure 30 shows the Bode plot for the impedance modulus for sol-gel-treated and painted AA6060 (sample 3dip-250) after the same number of

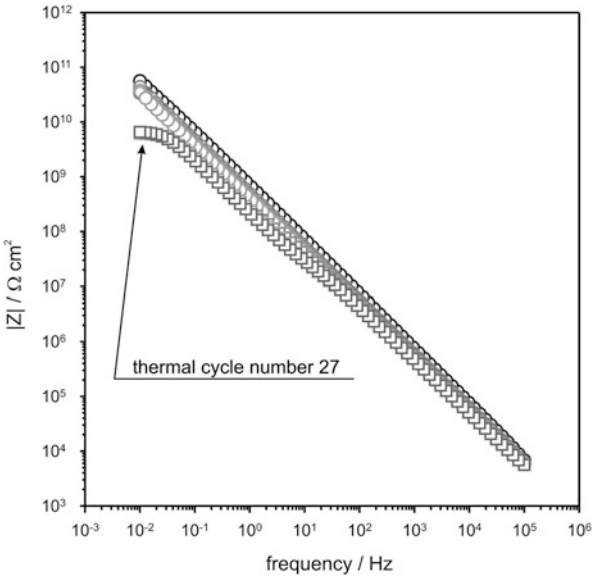

Fig. 29 Bode plot for impedance modulus for chromatized and topcoated AA6060 subjected to thermal cycles in 0.05% NaCl solution (Reprinted from Electrochim Acta, 52, Andreatta F, Aldighieri P, Paussa L, Di Maggio R, Rossi S, Fedrizzi L, Electrochemical behaviour of ZrO2 sol-gel pre-treatments on AA6060 aluminium alloy, 7545–7555, Copyright (2007), with permission from Elsevier)

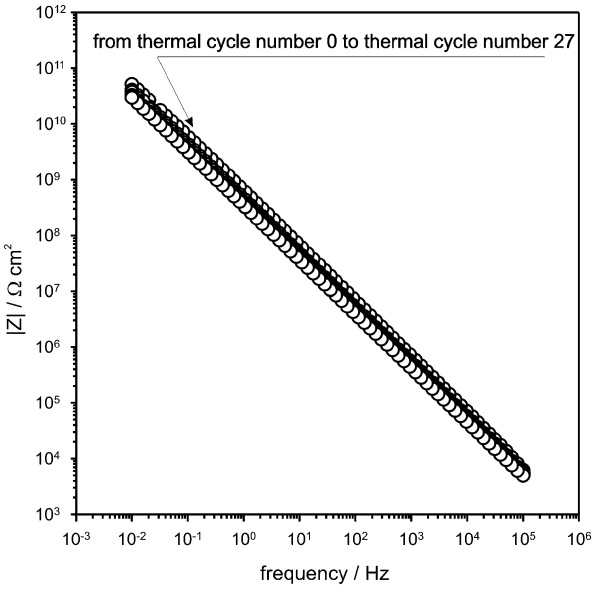

Fig. 30 Bode plot for impedance modulus for ZrO_2-pretreated (3dip-250) and topcoated AA6060 subjected to thermal cycles in 0.05% NaCl solution (Reprinted from Electrochim Acta, 52, Andreatta F, Aldighieri P, Paussa L, Di Maggio R, Rossi S, Fedrizzi L, Electrochemical behaviour of ZrO2 sol-gel pre-treatments on AA6060 aluminium alloy, 7545–7555, Copyright (2007), with permission from Elsevier)

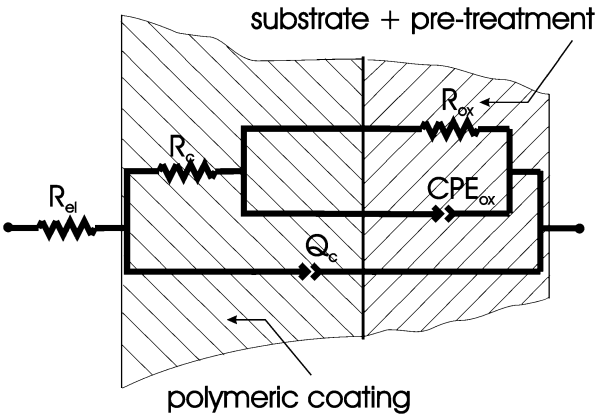

Fig. 31 Equivalent circuit to model pretreated samples topcoated with polyester spray resin (the thickness of the topcoat was 20 μm for all samples) (Reprinted from Electrochim Acta, 52, Andreatta F, Aldighieri P, Paussa L, Di Maggio R, Rossi S, Fedrizzi L, Electrochemical behaviour of ZrO2 sol-gel pre-treatments on AA6060 aluminium alloy, 7545–7555, Copyright (2007), with permission from Elsevier)

thermal cycles as in Fig. 29. The impedance modulus does not show any significant decrease after performing 27 thermal aging cycles.

Electrochemical impedance data obtained after thermal aging cycles are modeled using the equivalent circuit in Fig. 31. Q_c represents the nonideal capacitance of the topcoat, R_c is the ionic resistance of the topcoat through its intact or damaged

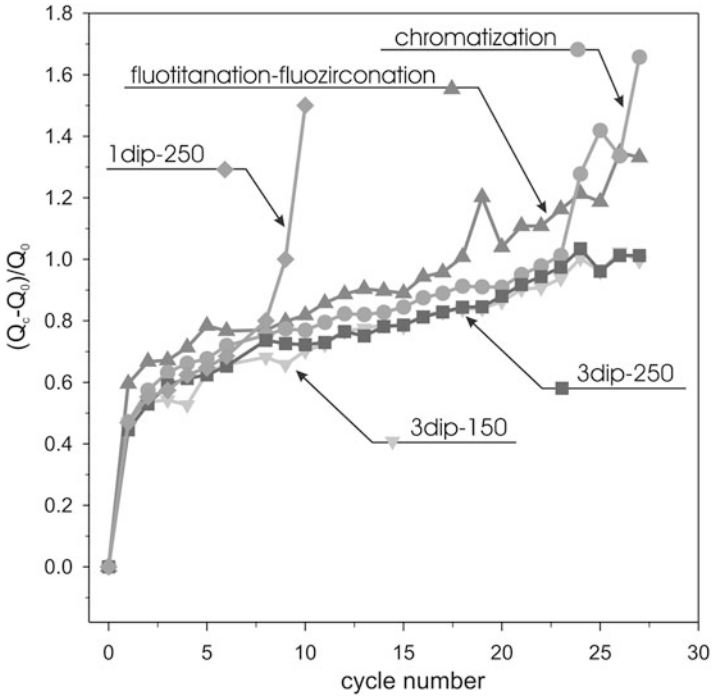

Fig. 32 Coating capacitance Q_c (normalized vs. the initial capacitance Q_0) as a function of thermal cycle number for chromatized AA6060, fluotitanated/fluozirconated AA6060, and ZrO_2-pretreated AA6060 (1dip-250, 3dip-150, and 3dip-250) (Reprinted from Electrochim Acta, 52, Andreatta F, Aldighieri P, Paussa L, Di Maggio R, Rossi S, Fedrizzi L, Electrochemical behaviour of ZrO2 sol-gel pre-treatments on AA6060 aluminium alloy, 7545–7555, Copyright (2007), with permission from Elsevier)

structure, and the constant phase element CPE_{ox} and the resistance R_{ox} describe the response of the pretreatment together with that of the substrate. This equivalent circuit was previously employed to describe the behavior of painted galvanized steel under thermal aging (Fedrizzi et al. 2006).

Figure 32 reports the coating capacitance Q_c normalized versus the initial capacitance as a function of the thermal aging cycle number for chromatized, fluotitanated/fluozirconated, and sol-gel-pretreated AA6060 (sample 3dip-250, 3dip-150, and 1dip-250). Three different phases can be distinguished for the behavior of Q_c of all samples characterized. An initial increase of Q_c (i) after the first thermal cycle is associated to not reversible solution ingress in the topcoat. This first increase of Q_c is significantly higher than the value reached at saturation when water uptake occurs at room temperature. Indeed, water can fill many microstructural and defect voids within paints including interfaces between pigments and polymer binder. Afterward, Q_c progressively increases due to further water uptake in the paint (ii). The last phase corresponds to a remarkable increase of Q_c (iii). This could correspond to the decrease of the electrochemical impedance modulus observed in Fig. 29. It is

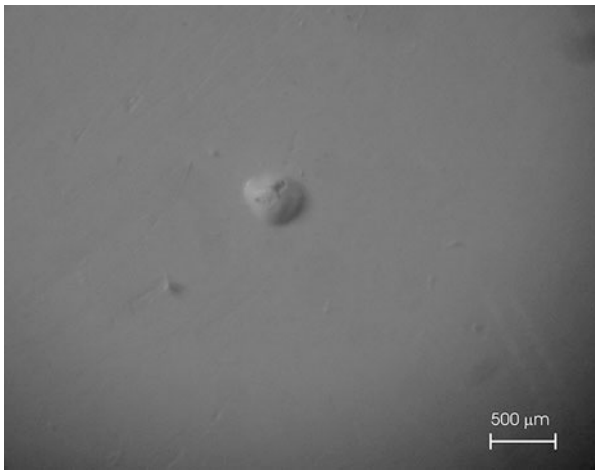

Fig. 33 Micrograph obtained with a stereo microscope on the surface of a chromatized and topcoated AA6060 after 27 thermal cycles (Reprinted from Electrochim Acta, 52, Andreatta F, Aldighieri P, Paussa L, Di Maggio R, Rossi S, Fedrizzi L, Electrochemical behaviour of ZrO2 sol-gel pre-treatments on AA6060 aluminium alloy, 7545–7555, Copyright (2007), with permission from Elsevier)

possible to correlate this clear increase of Q_c (iii) with blister formation and local loss of adhesion (Fedrizzi et al. 2006). As an example, Fig. 33 shows a blister on the surface of chromatized and painted AA6060 taken immediately after the electrochemical impedance measurement corresponding to thermal aging cycle 27. Besides, it was shown that samples that exhibit the large increase of Q_c after a relatively small number of thermal aging cycles are characterized by poor wet adhesion of the paint on the pretreated substrate (Fedrizzi et al. 2006).

It is well known that chromatized aluminum provides good adhesion to organic coatings. Therefore, the adhesion properties of sol-gel pretreatments and other conversion coatings have to be compared to that of chromatized AA6060. Fluotitanated/fluozirconated AA6060 exhibits a progressive degradation of Q_c. This is associated by a progressive increase of the slope of Q_c that is already evident after 18 thermal cycles. The morphology of fluotitanated/fluozirconated and painted AA6060 shows several blisters after 27 thermal aging cycles (not shown here). Hence, adhesion properties provided by fluotitanation/fluozirconation are less good than those of a chromate conversion coating, as well established in literature. Sample 3dip-250 and sample 3dip-150 do not exhibit a marked increase of Q_c, after 27 thermal cycles, and no blisters are visible on the surface of these samples. This behavior can be attributed to the limited number of defects observed for samples that underwent three successive depositions. This means that ZrO_2 pretreatments have a rather high resistance to water uptake and that there is very good wet adhesion of the topcoat to the substrate. Besides, the trend observed for sample 3dip-250 and sample 3dip-150 indicates that the wet adhesion properties are slightly better for ZrO_2 pretreatments that underwent thermal treatment at 150 °C than at 250 °C. This behavior could be most probably attributed to the existence of a higher content of organic and hydroxyl residuals in the sample heat treated at the lower temperature. This results in a structure with a higher content of bonding sites between ZrO_2 layer and topcoat. In contrast to samples that underwent three dips in the sol-gel solution

(sample 3dip-250 and sample 3dip-150), sample 1dip-250 shows a marked increase of Q_c after only after eight thermal cycles (Fig. 32) associated to the existence of a high amount of blisters and severe delamination (not shown here). The poor adhesion of the topcoat to the ZrO_2 pretreatment is caused by the defected structure of films obtained with only one dip in the sol-gel bath.

Critical Aspects in the Electrochemical Characterization of Sol-Gel Films

Potentiodynamic polarization measurements performed on sol-gel-coated aluminum alloys can provide information about the barrier properties of the pretreatment but do not enable the study of the modification of barrier properties as a function of immersion time. As shown in the examples above, this information can be achieved by electrochemical impedance spectroscopy. This method enables to assess barrier properties, adhesion behavior, and active corrosion protection in the case of sol-gel films with and without organic inhibitors. Moreover, it is also possible to investigate painted systems. This section focuses on some critical aspects related to the application of electrochemical techniques for the study of metal substrates coated with thin sol-gel films, which are, if properly deposited, defect-free films that can be considered an inert material. As a consequence, investigation of this inert material might generate critical aspects related to rapid fluctuations of its open circuit potential and current density during open circuit potential and potentiodynamic polarization measurements (Paussa et al. 2010a). Moreover, the unstable nature of the very thin sol-gel films is a critical issue also in electrochemical impedance measurements carried out under potential control because variation of the open circuit potential of the system during data acquisition might lead to sample damage. Impedance measurements under current control are an alternative method for data acquisition. This technique is considered in this section for the investigation of AA2024 substrate coated with a thin sol-gel layer and for chromate-conversion-coated alloy.

Electrochemical characterization of thin sol-gel films is often problematic due to difficulty to reach a steady-state condition. Moreover, properties of these systems are strongly dependent on deposition parameters. Therefore, surface reactivity of these systems might be affected by film defects, loss of adhesion, and possible formation of nano-cracks during immersion in an aggressive solution (Fedrizzi et al. 2001; Wang and Akid 2007). Figure 34 exhibits an example of a system that reaches a steady-state condition after an initial transient in the open circuit potential. This measurement was acquired in 0.05 M NaCl solution on chromate-conversion-coated AA2024. After an initial transient due to a passivation of the substrate, the chromate conversion coating provides continuous protection when immersed in the electrolyte. Immediately after immersion in the electrolyte, the open circuit potential exhibits a transient between −500 mV and −440 mV. This behavior is most likely associated to auto-repair mechanism due to Cr^{6+} species leading to an improvement of barrier properties. A steady-state condition is observed for longer immersion time.

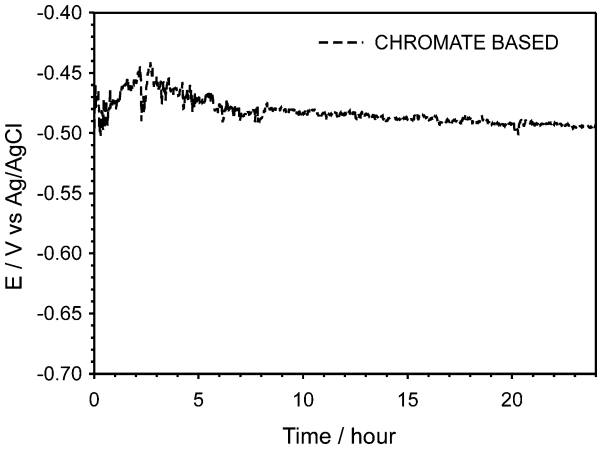

Fig. 34 Open circuit potential in 0.05 M NaCl for chromate-based coating deposited on AA2024 (Reprinted from Prog Org Coatings, 69, Paussa L, Andreatta F, Aldighieri P, Fedrizzi L, Critical aspects in the electrochemical study of unstable coated metallic substrates, 225–234, Copyright (2010a), with permission from Elsevier)

Therefore, we can assume that the chromate conversion coating becomes a stable system after 10 h of immersion in 0.05 M NaCl.

Figure 35 displays an example of a system that cannot be considered stationary. This is the case of AA2024 coated with a very thin ZrO_2 sol-gel film which is nearly defect-free. It can be expected that a significant variation of electrochemical behavior occurs when defects in ZrO_2 film are formed. In contrast with chromate conversion coating that is an auto-repair system, sol-gel ZrO_2 thin films are not able to restore the initial uniform protective layer after damage or corrosion attack. This means that no self-healing ability is observed for sol-gel ZrO_2 films. Plugging phenomena can occur due to formation of corrosion products inside film defects leading to a partial stabilization of the properties of ZrO_2 film. However, the protection provided in case of plugging phenomena is significantly lower relative to a defect-free film. Therefore, electrochemical behavior of ZrO_2 thin film is dependent on the quality of the deposited coating. Hence, it can be stated that ZrO_2 thin film can easily become an unstable system. Indeed, Fig. 35 shows that the open circuit potential in 0.05 M NaCl for sol-gel-coated AA2024 is not stable and exhibits strong oscillations during the entire measurement. The OCP evidences very fast oscillations in the range of 150 mV. This behavior can be associated to the deposition of an inert ZrO_2 film on a very reactive substrate like AA2024. In addition, the solution containing chlorides promotes meta-stable conditions, i.e., pitting corrosion. Open circuit potential oscillation visible in Fig. 35 is a critical aspect for electrochemical impedance spectroscopy since it is clearly recognizable that the alloy coated with a very thin ZrO_2 film does not show stationary behavior and can be considered as an unstable system.

As seen in this chapter, impedance measurements are often acquired on sol-gel films in order to follow the barrier properties of the coating as a function of the immersion time. This can be done with two different approaches consisting of potential or current control. The first approach is usually employed for impedance measurements of sol-gel films, as in the examples discussed in the previous sections. The second approach is discussed in detail in this section since it enables the

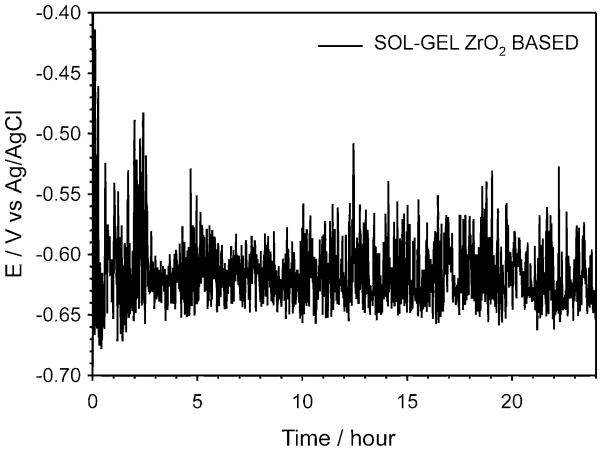

Fig. 35 Open circuit potential in 0.05 MNaCl for sol-gel ZrO_2-based coating deposited on AA2024 (Reprinted from Prog Org Coatings, 69, Paussa L, Andreatta F, Aldighieri P, Fedrizzi L, Critical aspects in the electrochemical study of unstable coated metallic substrates, 225–234, Copyright (2010a), with permission from Elsevier)

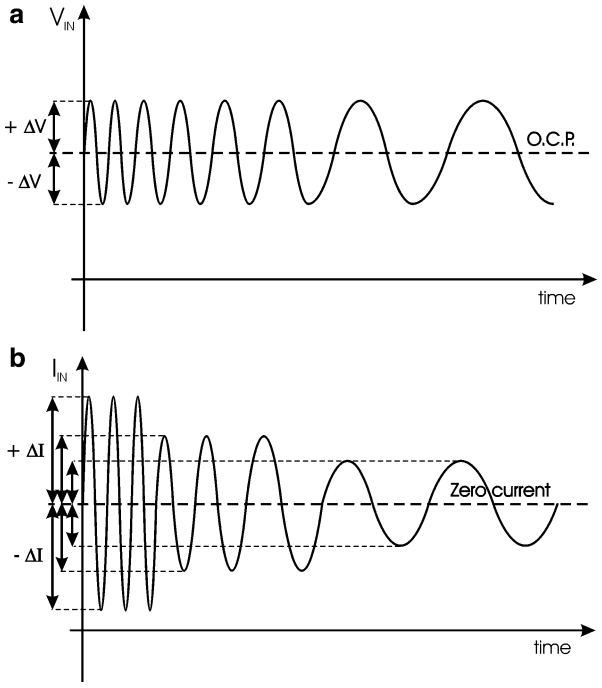

Fig. 36 Schemes of input signal for impedance measurements under voltage control (**a**) and current control (**b**) for a stable system (Reprinted from Prog Org Coatings, 69, Paussa L, Andreatta F, Aldighieri P, Fedrizzi L, Critical aspects in the electrochemical study of unstable coated metallic substrates, 225–234, Copyright (2010a), with permission from Elsevier)

acquisition of impedance data for systems with nonstationary behavior, as for the sol-gel film presented in Fig. 35. Figure 36a displays the input signal (V_{IN}) for impedance measurements under voltage control. A voltage input perturbation with an amplitude of 10 mV is applied to the system at the open circuit potential. This open circuit potential is measured for 60 s before acquisition of impedance data. The open circuit potential measured after 60 s represents the mean value of input sine

wave voltage perturbation for the successive EIS measurements. Under potential control, a constant sine wave amplitude is applied during the frequency scan. Figure 36b shows the input signal (I_{IN}) for impedance measurements under current control. These measurements are carried out imposing a ΔI perturbation at a finite direct current value. The mean value of the sine wave corresponds to a current that is equal to zero (Fig. 36b). This current is directly correlated to the open circuit potential of the system. The perturbation signal changes in amplitude because the impedance measurements carried out under current control have to ensure the linear response of the system maintaining the output (V_{OUT}) below 10 mV (Paussa et al. 2010a).

The open circuit potential is the mean value for the sine wave under voltage control (Fig. 36a) while the zero current condition is the mean value under current control (Fig. 36b). Since the open circuit potential is the value of the potential for which the net current of redox processes is equal to zero, measurements under current control must give the same response of those carried out under potential control. An example is given in Fig. 37, which shows Bode module and phase angle plots for impedance measurement performed on AA2024 coated with chromate conversion coating in 0.05 M NaCl under voltage and current control. These measurements have been carried out after 72 h of immersion in order to have stationary conditions for the open circuit potential. In the case of a stable system, it can be seen that the plots of impedance modulus and phase angle overlap for the two systems. This indicates that measurements carried out under current and voltage control lead to the same system response in the case of stable sample.

Figure 38 reports a scheme for impedance measurements associated to voltage and current control in the case of the unstable system like the sol-gel-coated AA2024 presented in Fig. 35. In the example in Fig. 38a, the open circuit potential becomes more negative during the impedance measurement. A mean value of sine wave corresponding to open circuit potential measured after 60 s immersion times is

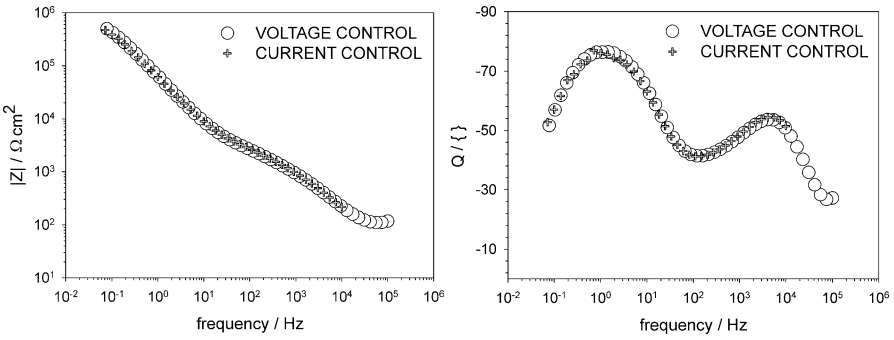

Fig. 37 Bode plots of impedance module and phase angle for AA2024 coated with chromate-based coating in 0.05 M NaCl. Impedance measurements were carried out under voltage and current control (Reprinted from Prog Org Coatings, 69, Paussa L, Andreatta F, Aldighieri P, Fedrizzi L, Critical aspects in the electrochemical study of unstable coated metallic substrates, 225–234, Copyright (2010a), with permission from Elsevier)

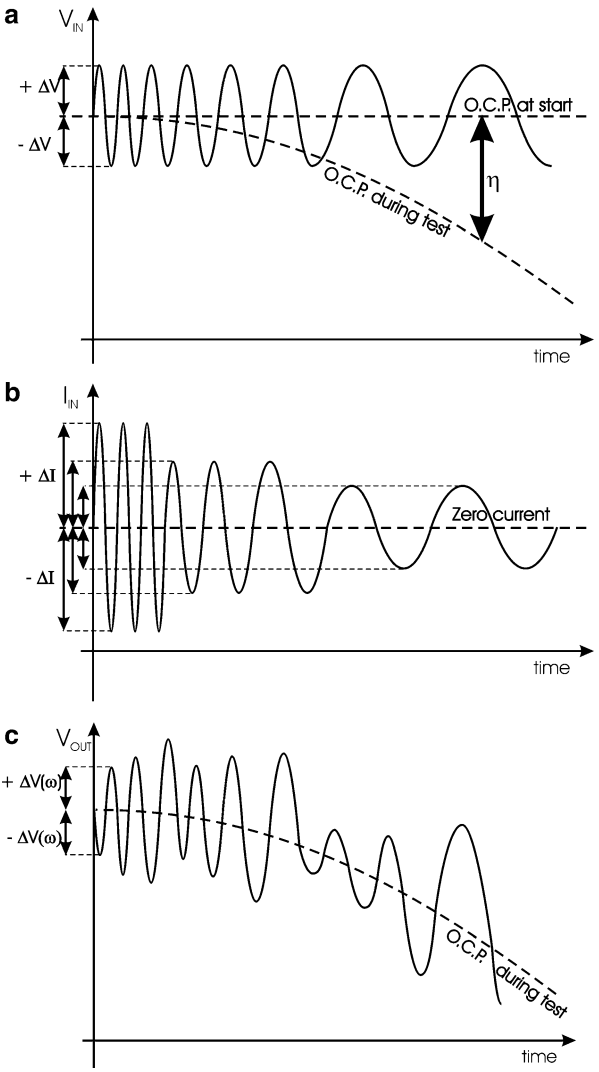

Fig. 38 Schemes of input signal for impedance measurements under voltage control (**a**) and current control (**b**) for an unstable system. The output signal is also reported for measurements performed under current control on unstable system (**c**) (Reprinted from Prog Org Coatings, 69, Paussa L, Andreatta F, Aldighieri P, Fedrizzi L, Critical aspects in the electrochemical study of unstable coated metallic substrates, 225–234, Copyright (2010a), with permission from Elsevier)

imposed under voltage control when the impedance measurement is started. This value is maintained constant during the entire measurement. Since the open circuit potential of the system is changing during the test, the sample is polarized at an anodic overpotential (η). In particular, the extent of the polarization becomes significant at low frequency because the potential shift might be rather large due to the duration of the measurement. Therefore, the instability of the system will impair the impedance measurement. In addition, anodic polarization of the sample at low frequency might lead to extensive damage of the sample. As a consequence, it is not possible to obtain reliable information for impedance measurements carried out under voltage control on unstable systems since the measurements cause accelerated

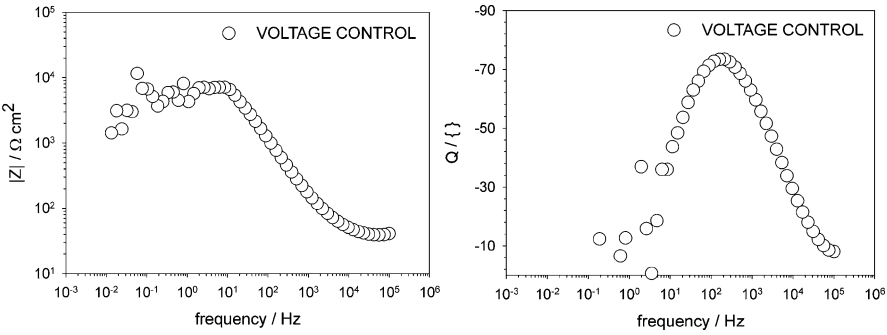

Fig. 39 Bode plots of impedance module and phase angle for AA2024 coated with sol-gel ZrO_2 thin film in 0.05 MNaCl. The impedance measurement was carried out under voltage control (Reprinted from Prog Org Coatings, 69, Paussa L, Andreatta F, Aldighieri P, Fedrizzi L, Critical aspects in the electrochemical study of unstable coated metallic substrates, 225–234, Copyright (2010a), with permission from Elsevier)

degradation of the coating. An example is given in Fig. 39, which shows an impedance measurement under voltage control for AA2024 coated with a sol-gel ZrO_2 thin film after 1 h of immersion in 0.05 M NaCl solution. The trend of impedance modulus and phase angle in Fig. 39 clearly shows an evident instability in the spectrum for frequencies lower than 10 Hz. The impedance measurement cannot be validated in this case, and no reliable information can be obtained about the system under investigation.

Figure 38b shows a scheme of the input signal for an impedance measurement under current control for the unstable system. The trend of the input signal is the same as for that shown in Fig. 36b for the stable system. As already observed, the mean value of current perturbation corresponds to the condition of zero current. However, the amplitude of the oscillations is not constant during the measurements because the impedance response of the system is a function of the input signal frequency. Therefore, the input signal must be carefully selected during impedance measurements carried out under current control. The detailed description of the procedure followed for measurements under current control is beyond the scope of this chapter (Paussa et al. 2010a). However, it is important to point out that the main advantage of measurements under current control is that the output signal follows the variation of the open circuit potential, as shown in Fig. 38c. This guarantees the stability condition during the entire impedance scan. In the case of unstable systems, this approach preserves the sample from degradation due to the possible overpotentials which can be applied in the case of measurements under voltage control.

Figure 40 displays the Bode module and phase angle plots after 24 h of immersion in 0.05 M NaCl on AA2024 coated with a sol-gel ZrO_2 thin film. This measurement was carried out under current control imposing a zero current condition for 20 s before each frequency scan. The Bode plot for impedance module does not show discontinuities that were observed for the measurements under potential

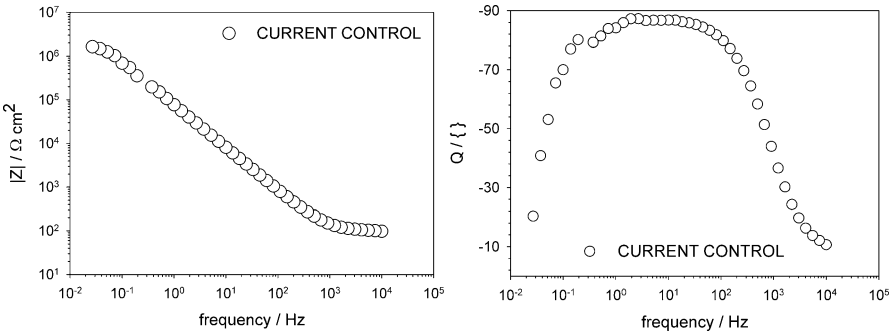

Fig. 40 Bode plots of impedance module and phase angle for AA2024 coated with sol-gel ZrO_2 thin film after 24 h of immersion in 0.05 M NaCl. The impedance measurement was carried out under current control (Reprinted from Prog Org Coatings, 69, Paussa L, Andreatta F, Aldighieri P, Fedrizzi L, Critical aspects in the electrochemical study of unstable coated metallic substrates, 225–234, Copyright (2010a), with permission from Elsevier)

control. In general, it can be stated that accuracy of the measurement is very good and that the linearity of the system is preserved during the measurement since the sample is not polarized during the impedance measurement. The absence of sample damage guaranteed under current control enables to study the evolution of the system as a function of immersion time in the solution. This information is not accessible by means of impedance measurements under voltage control on these unstable systems.

Conclusion

The use of the electrochemical techniques for the characterization of sol-gel-coated metals has been considered in this chapter. Potentiodynamic polarization measurements can be used to assess barrier properties of sol-gel films. Open circuit potential measurements and electrochemical impedance spectroscopy are suitable for the investigation of the corrosion behavior of the sol-gel-coated metals for long immersion times in aggressive electrolytes. The combinatorial use of the electrochemical techniques considered in this chapter can provide useful information about corrosion behavior and durability of sol-gel-coated metals. Some critical aspects related to the use of electrochemical methods are evidenced in the case of sol-gel-coated metals due to the unstable electrochemical behavior of the sol-gel films. Electrochemical impedance measurements carried out under current control can overcome most of these issues.

Acknowledgments The authors would like to kindly acknowledge all coauthors of the papers discussed in this chapter. A special mention goes to P. Aldighieri, L. Paussa, and A. Lanzutti, who strongly contributed to the acquisition and discussion of the experimental data presented in this work. Part of the results in this paper and the work it concerns were generated in the context of the MULTIPROTECT project, funded by the European Community as Contract No. NMP3-CT-2005-011783 under

the 6th Framework Programme for Research and Technological Development. The project partners that contributed to the results presented in this chapter are kindly acknowledged. In particular, the authors would like to thank A. Duran, M. Aparicio, and their coworkers for the collaboration in the framework of the MULTIPROTECT project.

References

Andreatta F, Aldighieri P, Paussa L, Di Maggio R, Rossi S, Fedrizzi L. Electrochemical behaviour of ZrO_2 sol–gel pre-treatments on AA6060 aluminium alloy. Electrochim Acta. 2007;52(27 Special Issue):7545–55.

Andreatta F, Paussa L, Aldighieri P, Lanzutti A, Fedrizzi L. ZrO_2 pre-treatments deposited with sol–gel technique on aluminium alloys. 17th International Corrosion Congress 2008: Corrosion Control in the Service of Society; 2008.

Andreatta F, Paussa L, Aldighieri P, Lanzutti A, Raps D, Fedrizzi L. Corrosion behaviour of sol–gel treated and painted AA2024 aluminium alloy. Prog Org Coat. 2010a;69(2):133–42.

Andreatta F, Paussa L, Aldighieri P, Lanzutti A, Ondratschek D, Fedrizzi L. Water-based ZrO_2 pretreatment for AA2024 aluminum alloy. Surf Interface Anal. 2010b;42(4):293–8.

Andreatta F, Paussa L, Lanzutti A, Rosero Navarro NC, Aparicio M, Castro Y, et al. Development and industrial scale-up of ZrO_2 coatings and hybrid organic-inorganic coatings used as pre-treatments before painting aluminium alloys. Prog Org Coat. 2011;72(1–2):3–14.

Arnott DR, Hinton BRW, Ryan NE. Cationic film-forming inhibitors for the corrosion protection of AA7075 aluminum alloy in chloride solutions. Mater Perform. 1987;26(8):42–7.

Ballard RL, Williams JP, Njus JM, Kiland BR, Soucek MD. Inorganic-organic hybrid coatings with mixed metal oxides. Eur Polym J. 2001;37(2):381–98.

Bard J, Faulkner LR. Electrochemical methods: fundamentals and applications. 2nd ed. New York: Wiley; 2001.

Beccaria AM, Chiaruttini L. The inhibitive action of metacryloxypropylmethoxysilane (MAOS) on aluminium corrosion in NaCl solutions. Corros Sci. 1999;41(5):885–99.

Beccaria AM, Padeletti G, Montesperelli G, Chiaruttini L. The effect of pretreatments with siloxanes on the corrosion resistance of aluminium in NaCl solution. Surf Coat Technol. 1999;111(2–3):240–6.

Bethencourt M, Botana FJ, Calvino JJ, Marcos M, Rodríguez-Chacón MA. Lanthanide compounds as environmentally-friendly corrosion inhibitors of aluminium alloys: a review. Corros Sci. 1998;40(11):1803–19.

Campestrini P, Terryn H, Vereecken J, De Wit JHW. Chromate conversion coating on aluminum alloys III. Corrosion protection. J. Electrochem Soc. 2004;151(6):B370–B377.

Di Maggio R, Fedrizzi L, Rossi S. Effect of the chemical modification of the precursor of ZrO_2 films on the adhesion of organic coatings. J Adhes Sci Technol. 2001;15(7):793–808.

Fedrizzi L, Rodriguez FJ, Rossi S, Deflorian F, Di Maggio R. Initial and later stages of anodic oxide formation on Cu, chemical aspects, structure and electronic properties. Electrochim Acta. 2001;46(24–25):3755–66.

Fedrizzi L, Bergo A, Fanicchia M. Evaluation of accelerated aging procedures of painted galvanised steels by EIS. Electrochim Acta. 2006;51(8–9):1864–72.

Fontana MG. Corrosion engineering. 3rd ed. New York: McGraw-Hill; 1986.

Galio AF, Lamaka SV, Zheludkevich ML, Dick LFP, Müller IL, Ferreira MGS. Inhibitor-doped sol–gel coatings for corrosion protection of magnesium alloy AZ31. Surf Coat Technol. 2010;204(9–10):1479–86.

Goeminne G, Terryn H, Vereecken J. Characterisation of conversion layers on aluminium by means of electrochemical impedance spectroscopy. Electrochim Acta. 1995;40(4):479–486.

Guglielmi M. Sol–Gel coatings on metals. J Sol Gel Sci Technol. 1997;8(1–3):443–9.

Hughes AE, Taylor RJ, Hinton BRW, Wilson L. XPS and SEM characterization of hydrated cerium oxide conversion coatings. Surf Interface Anal. 1995;23(7–8):540–50.

Iannuzzi M, Kovac J, Frankel GS. A study of the mechanisms of corrosion inhibition of AA2024-T3 by vanadates using the split cell technique. Electrochim Acta. 2007;52(12):4032–42.
Ilevbare GO, Scully JR. Oxygen reduction reaction kinetics on chromate conversion coated Al-Cu, Al-Cu-Mg, and Al-Cu-Mn-Fe intermetallic compounds. J Electrochem Soc. 2001;148(5): B196–207.
Kelly RG, Scully JR, Shoesmith DW, Buchheit RG. Electrochemical techniques in corrosion science and engineering. New York: Marcel Dekker; 2002.
Kendig MW, Buchheit RG. Corrosion inhibition of aluminum and aluminum alloys by soluble chromates, chromate coatings, and chromate-free coatings. Corrosion. 2003;59(5):379–400.
Khramov AN, Voevodin NN, Balbyshev VN, Donley MS. Hybrid organo-ceramic corrosion protection coatings with encapsulated organic corrosion inhibitors. Thin Solid Films. 2004;447–448:549–57.
Magalhães AAO, Margarit ICP, Mattos OR. Molybdate conversion coatings on zinc surfaces. J Electroanal Chem. 2004;572(2):433–40.
Mansfeld F, Lin S, Kim S, Shih H. Pitting and passivation of Al alloys and Al-based metal matrix composites. J Electrochem Soc. 1990;137(1):78–82.
Metroke TL, Apblett A. Effect of solvent dilution on corrosion protective properties of Ormosil coatings on 2024-T3 aluminum alloy. Prog Org Coat. 2004;51(1):36–46.
Metroke TL, Parkhill RL, Knobbe ET. Passivation of metal alloys using sol–gel-derived materials – a review. Prog Org Coat. 2001;41(4):233–8.
Osborne JH. Observations on chromate conversion coatings from a sol–gel perspective. Prog Org Coat. 2001;41(4):280–6.
Osborne JH, Blohowiak KY, Taylor SR, Hunter C, Bierwagon G, Carlson B, et al. Testing and evaluation of nonchromated coating systems for aerospace applications. Prog Org Coat. 2001;41(4):217–25.
Paussa L, Andreatta F, Aldighieri P, Fedrizzi L. Critical aspects in the electrochemical study of unstable coated metallic substrates. Prog Org Coat. 2010a;69(2):225–34.
Paussa L, Rosero-Navarro NC, Andreatta F, Castro Y, Duran A, Aparicio M, et al. Inhibition effect of cerium in hybrid sol–gel films on aluminium alloy AA2024. Surf Interface Anal. 2010b;42 (4):299–305.
Paussa L, Rosero Navarro NC, Bravin D, Andreatta F, Lanzutti A, Aparicio M, et al. ZrO_2 sol–gel pre-treatments doped with cerium nitrate for the corrosion protection of AA6060. Prog Org Coat. 2012;74(2):311–9.
Ramsey JD, McCreery RL. In situ Raman microscopy of chromate effects on corrosion pits in aluminum alloy. J Electrochem Soc. 1999;146(11):4076–81.
Rosero-Navarro NC, Pellice SA, Durán A, Aparicio M. Effects of Ce-containing sol–gel coatings reinforced with SiO_2 nanoparticles on the protection of AA2024. Corros Sci. 2008;50 (5):1283–91.
Rosero-Navarro NC, Paussa L, Andreatta F, Castro Y, Durán A, Aparicio M, et al. Optimization of hybrid sol–gel coatings by combination of layers with complementary properties for corrosion protection of AA2024. Prog Org Coat. 2010;69(2):167–74.
Sheir LL, Jarman RA, Burstein GT. Corrosion, vol. 1–2. 3rd ed. Oxford: Butterworth-Heinemann; 1994.
Tang L, Li X, Si Y, Mu G, Liu G. The synergistic inhibition between 8-hydroxyquinoline and chloride ion for the corrosion of cold rolled steel in 0.5 M sulfuric acid. Mater Chem Phys. 2006;95(1):29–38.
Twite RL, Bierwagen GP. Review of alternatives to chromate for corrosion protection of aluminum aerospace alloys. Prog Org Coat. 1998;33(2):91–100.
Voevodin NN, Grebasch NT, Soto WS, Arnold FE, Donley MS. Potentiodynamic evaluation of sol–gel coatings with inorganic inhibitors. Surf Coat Technol. 2001;140(1):24–8.
Voevodin NN, Balbyshev VN, Donley MS. Investigation of corrosion protection performance of sol–gel coatings on AA2024-T3. Prog Org Coat. 2005;52(1 Special Issue):28–33.

Wang H, Akid R. A room temperature cured sol–gel anticorrosion pre-treatment for Al 2024-T3 alloys. Corros Sci. 2007;49(12):4491–503.

Xia L, Akiyama E, Frankel G, McCreery R. Storage and release of soluble hexavalent chromium from chromate conversion coatings. Equilibrium aspects of CrVI concentration. J Electrochem Soc. 2000;147(7):2556–62.

Yang H, Van Ooij WJ. Plasma-treated triazole as a novel organic slow-release paint pigment for corrosion control of AA2024-T3. Prog Org Coat. 2004;50(3):149–61.

Yang XF, Tallman DE, Gelling VJ, Bierwagen GP, Kasten LS, Berg J. Use of a sol–gel conversion coating for aluminum corrosion protection. Surf Coat Technol. 2001;140(1):44–50.

Yasakau KA, Zheludkevich ML, Lamaka SV, Ferreira MGS. Mechanism of corrosion inhibition of AA2024 by rare-earth compounds. J Phys Chem B. 2006;110(11):5515–28.

Yasakau KA, Zheludkevich ML, Karavai OV, Ferreira MGS. Influence of inhibitor addition on the corrosion protection performance of sol–gel coatings on AA2024. Prog Org Coat. 2008;63 (3):352–61.

Zhao J, Frankel G, McCreery RL. Corrosion protection of untreated AA-2024-T3 in chloride solution by a chromate conversion coating monitored with Raman spectroscopy. J Electrochem Soc. 1998;145(7):2258–64.

Zheludkevich ML, Serra R, Montemor MF, Yasakau KA, Salvado IMM, Ferreira MGS. Nanostructured sol–gel coatings doped with cerium nitrate as pre-treatments for AA2024-T3 Corrosion protection performance. Electrochim Acta. 2005a;51(2):208–17.

Zheludkevich ML, Yasakau KA, Poznyak SK, Ferreira MGS. Triazole and thiazole derivatives as corrosion inhibitors for AA2024 aluminium alloy. Corros Sci. 2005b;47(12):3368–83.

Zheludkevich ML, Serra R, Montemor MF, Miranda Salvado IM, Ferreira MGS. Corrosion protective properties of nanostructured sol–gel hybrid coatings to AA2024-T3. Surf Coat Technol. 2006;200(9):3084–94.